4 Tribological evaluation of mineral oil–based greases

This chapter covers the detailed characterization of nanoadditives used in the present study. The crystalline and morphological features of MoS_2, MoS_2–ODT, GO, rGO, and GO–ODA nanoadditives were probed by XRD and HRTEM analyses. FTIR analysis confirmed the synthesis and chemical functionalization of nanoadditives. The paraffin grease was formulated using paraffin oil as a base oil and 12–lithium hydroxystearate metallic soap as a thickener. The chapter discusses the tribological performance of mineral oil–based grease with and without nanoadditives. Tribological test results unveiled the role of nanoadditives on the lubrication performance of the paraffin grease.

4.1 Characterization of MoS_2 and MoS_2–ODT nanosheets

XRD analysis demonstrated the crystalline characteristics of MoS_2 and MoS_2–ODT nanosheets. **Figure 4.1a** shows XRD peaks of MoS_2 nanosheets over the 2θ range of 10–80°. The MoS_2 nanosheets exhibited characteristics diffraction peaks of MoS_2 at 2θ of 14.2°, 33°, 39°, 58.7° and 69.3° corresponding to (002), (101), (103), (110) and (201) planes, respectively. Furthermore, these peaks are fully matched with JCPDS data card No 75–1539 of MoS_2. The diffraction pattern of MoS_2–ODT nanosheets (**Figure 4.1b**) is indistinguishable from the characteristic's diffraction peaks of MoS_2, which suggests that the crystalline features of MoS_2 nanosheets are not affected by the functionalization with ODT. However, MoS_2–ODT nanosheets exhibited few diffraction peaks in the 2θ range of 19 to 25°, which are under investigation. The diffraction peak at 2θ of 14.2° corresponding to (002) basal plane signified the highly ordered stacking of molecular lamellae of MoS_2 with an estimated interlayer spacing of 0.623 nm.

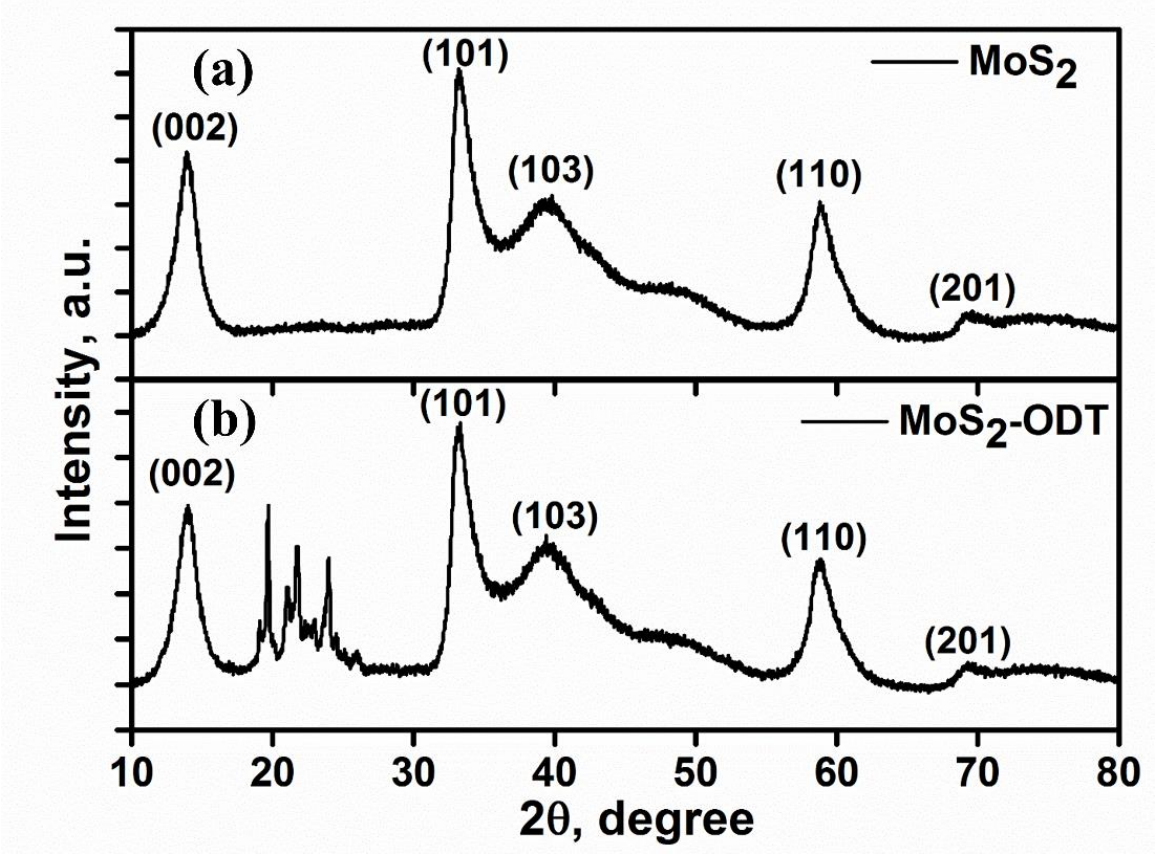

Figure 4.1: X–ray diffraction patterns (a) MoS_2 and (b) MoS_2–ODT nanosheets

The FTIR spectroscopic measurements affirmed the functionalization of MoS_2 with ODT. **Figure 4.2** depicts FTIR vibrational spectra of MoS_2 and MoS_2–ODT nanosheets along with vibrational assignments of their characteristic peaks. The vibrational peak at 510 cm^{-1} is attributed to Mo–S stretching mode and confirmed the formation of MoS_2 nanosheets (Nagaraju et al., 2007). The strong vibrational peak at ~1650 cm^{-1} is assigned to the bending mode of water molecules. The MoS_2 synthesized by a hydrothermal approach exhibited defect sites, which could be due to the absorption of the water molecules (Finnie et al., 2001). The emergence of strong vibrational features in the range of 2800 to 3000 cm^{-1} due to methylene and methyl asymmetric and symmetric stretching modes (d^-, d^+, r^-, r^+) revealed the grafting of octadecanethiol on the MoS_2 nanosheets. Furthermore, the bending vibrations at 1467 and 718 cm^{-1} are ascribed to the scissoring and rocking modes of methylene units of ODT grafted on the MoS_2 nanosheets.

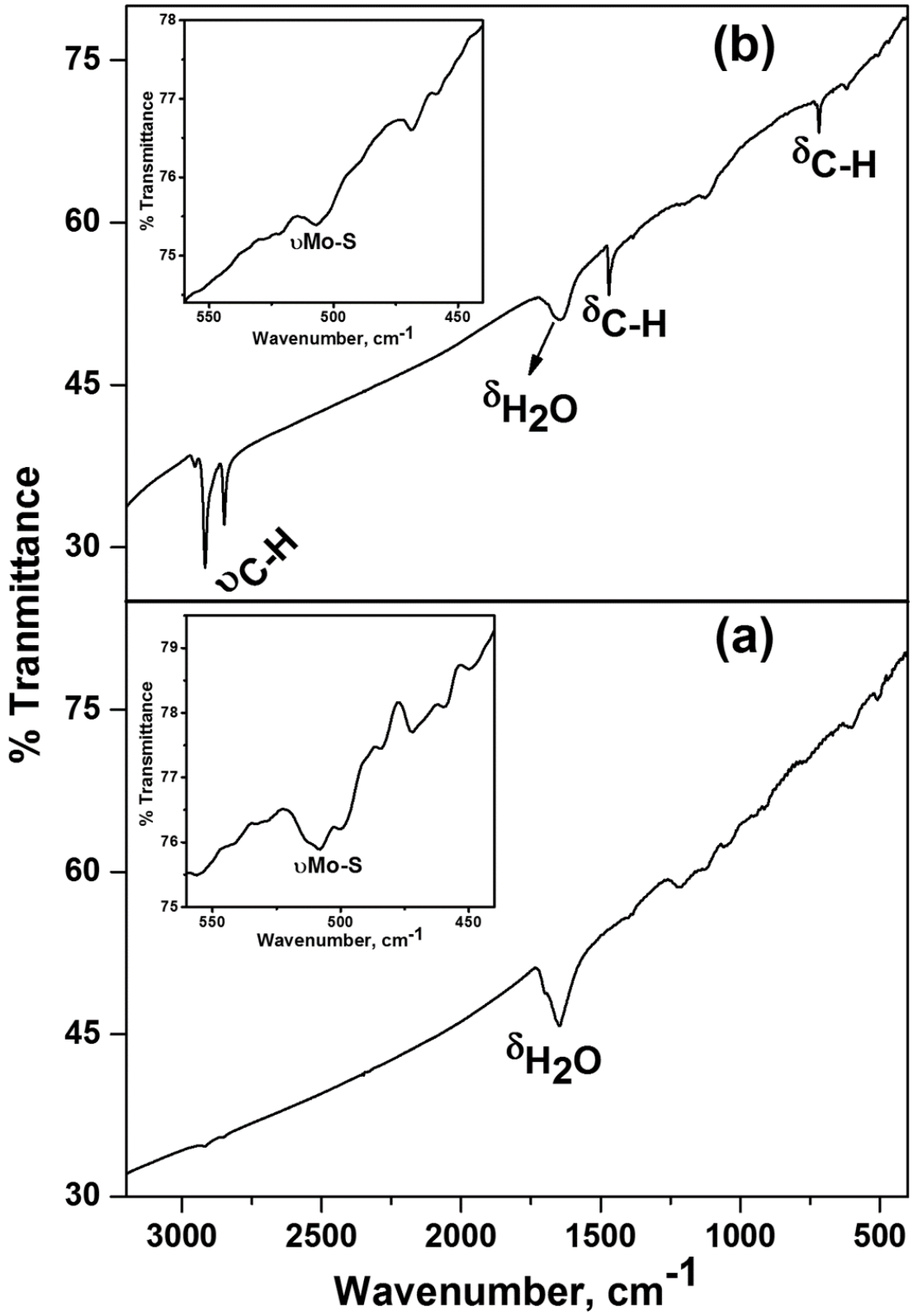

Figure 4.2: FTIR spectra (a) MoS_2 and (b) MoS_2–ODT nanosheets along with the vibrational features

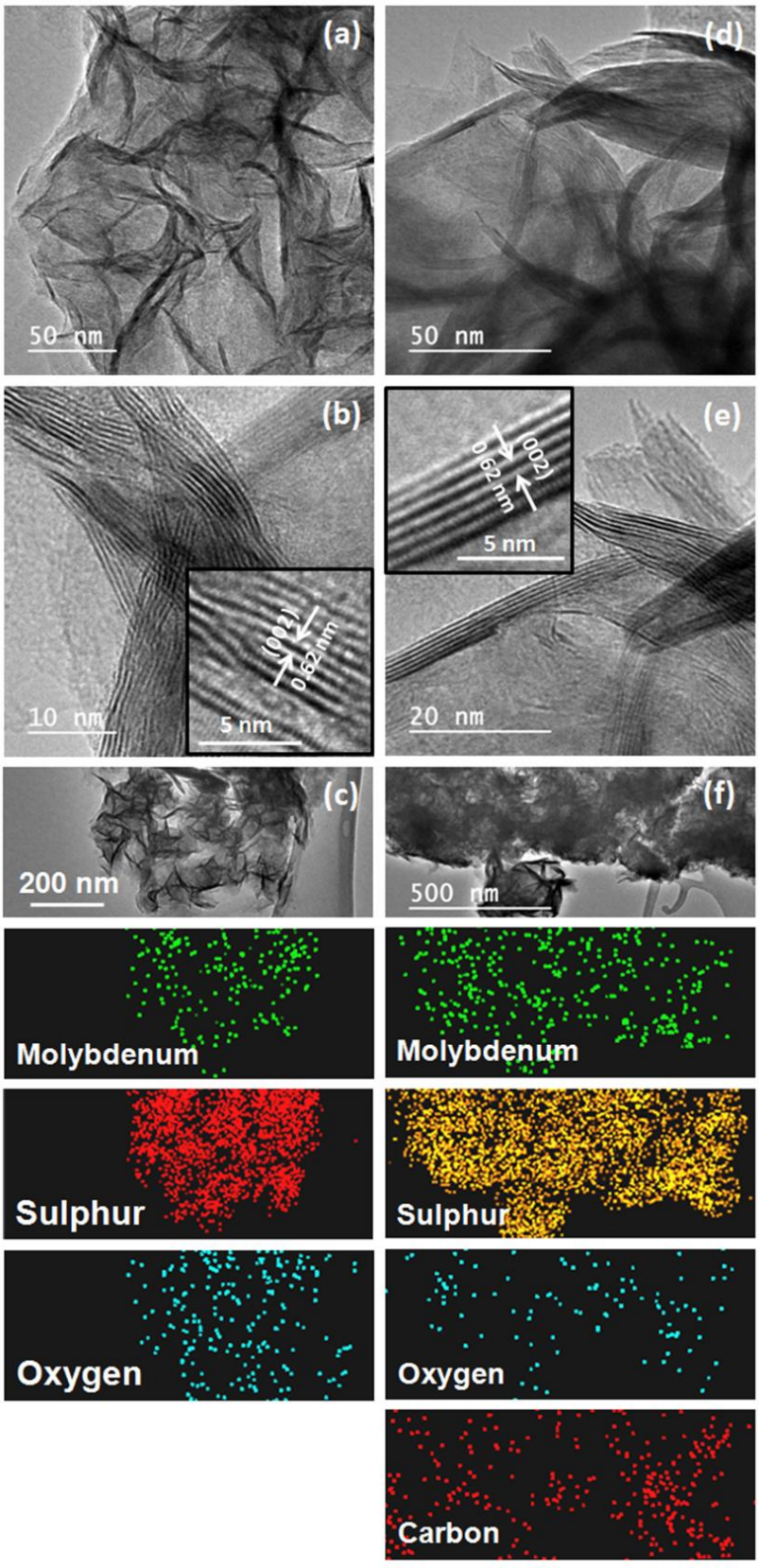

Figure 4.3: Low and high resolutions TEM images of (a–b) MoS_2 and (d–e) MoS_2–ODT nanosheets. TEM micrographs of (c) MoS_2 and (f) MoS_2–ODT along with corresponding area elemental mapping. The lamellar structure of MoS_2 along with interlayer spacing is explicitly seen in high–resolution images

HRTEM analysis revealed the nanostructural features of MoS_2 and MoS_2–ODT nanosheets. **Figure 4.3a–f** displays the TEM images of MoS_2 and MoS_2–ODT nanosheets at variable magnifications. The low–resolution images (**Figure 4.3a,d**) explicitly show the aggregates of hair–like thin sheets of MoS_2 and MoS_2–ODT. The individual sheet of MoS_2 and MoS_2–ODT is found to be made of 4–12 thick molecular lamellae, as revealed from their high–resolution TEM images (**Figure 4.3b,e**). The van der Waals interaction between the molecular lamellae of MoS_2 holds them together with the interlayer spacing of 0.62 nm, close to the characteristic interlayer spacing of 0.616 nm for the (002) plane of MoS_2 (Gan et al., 2018). The microstructure of MoS_2 nanosheets remained intact, including interlamellar spacing after functionalization with ODT. It suggests that ODT molecules are tethered on the surface sites of MoS_2 nanosheets. The elemental mappings of MoS_2 and MoS_2–ODT nanosheets were examined using the EDS to confirm the grafting of ODT. The TEM micrograph (**Figure 4.3c**) along with corresponding area elemental distribution (Mo and S) affirmed the MoS_2 nanosheets. The distribution of oxygen indicates the oxygen sites in the form of MoO_3 traces in MoS_2 nanosheets. The lower coordinated sites of Mo and defects in the MoS_2 nanosheets are susceptible to oxygen substitution (Liang et al., 2011). As a result, oxygen sites are accumulated on the surface of MoS_2 nanosheets, particularly when they are prepared by a hydrothermal approach. The TEM images (**Figure 4.3f**) and corresponding area elemental distribution of MoS_2–ODT displayed the regular distribution of carbon besides Mo, S, and O, confirming the grafting of octadecanethiol on the MoS_2 nanosheets.

4.2 Characterization of GO, rGO, and GO–ODA nanosheets

Figure 4.4 shows the XRD patterns of GO, rGO, and GO–ODA. The diffraction pattern of GO exhibited a characteristic peak at 2θ of 10.94°, revealing the interlayer spacing of 0.81

nm between adjacent atomic lamella. The presence of ample oxygen functionalities and trapped water molecules made GO hydrophilic and increased the interlamellar spacing (0.81 nm) compared to graphene (0.34 nm). The reduction of GO eliminated most oxygen functionalities and restored the characteristic interlamellar spacing of graphene (Choudhary et al., 2012; Mungse and Khatri, 2014; G. Wang et al., 2008). Therefore, the XRD peak of (002) plane shifted towards a higher 2θ of 25.50° and revealed the interlayer spacing of 0.35 nm in the rGO (**Figure 4.4**). The broadness of the XRD peak suggests that rGO nanosheets are made of a limited number of lamellae, grouped in a random order, and exhibited comparatively poor crystalline structure, particularly in the basal plane compared to that of graphene. The chemical functionalization of GO by grafting of ODA showed significant changes in the XRD pattern. The GO–ODA exhibited a major characteristic peak at 2θ of 21.32°, corresponding to the interlamellar spacing of 0.42 nm, larger than that of the rGO. The larger interlamellar spacing (0.42 nm) in GO–ODA is ascribed to the presence of residual oxygen functionalities (Mungse et al., 2015). The amino functionality of ODA molecules is interacted with basal plane oxygen functionalities and formed the GO–ODA. As a result, interlamellar spacing in GO greatly expanded to 1.68 and 3.30 nm, as revealed by corresponding XRD peaks at 2θ of 5.25° and 2.68°, respectively. The grafting density within the basal plane, the orientation of ODA molecules, and the van der Waals interaction between the octadecyl chains governed the interlamellar spacing in the GO–ODA (Mungse et al., 2015).

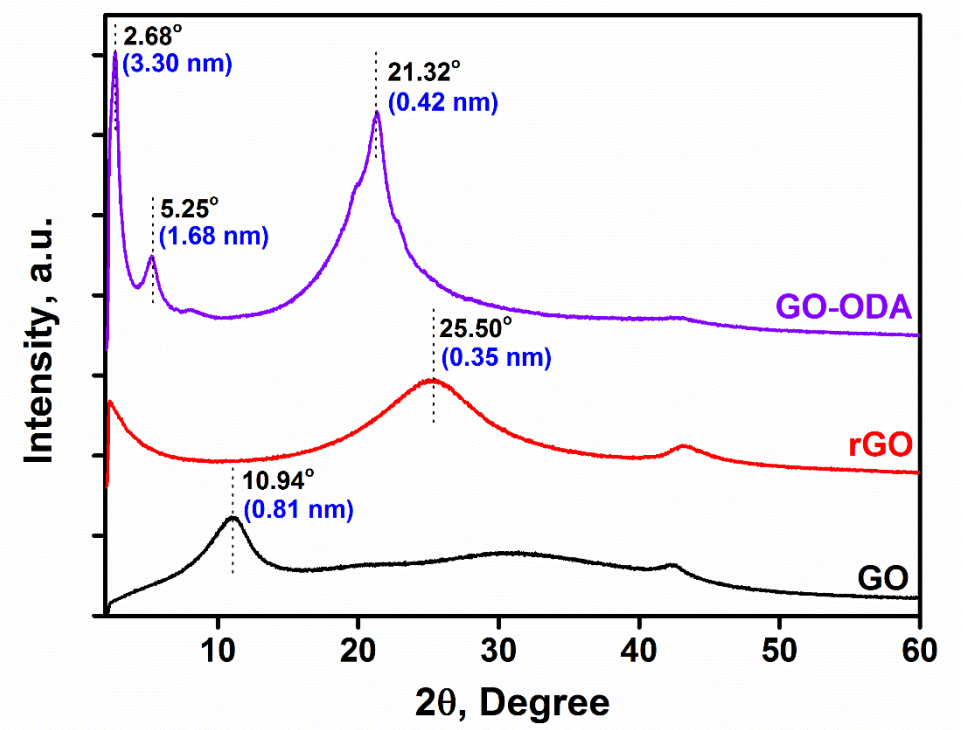

Figure 4.4: XRD patterns of GO, rGO, and GO–ODA nanosheets

The FTIR spectra of GO, rGO, and GO–ODA is depicted in **Figure 4.5**. The characteristics vibrational peaks of GO at 1724, 1616, 1375, 1250, and 1055 cm^{-1} are assigned to υC=O (stretching mode of carboxylic groups), υC=C (in–plane stretching of sp^2–hybridized carbon along with bending mode of H_2O molecules), δOH (bending of hydroxyl groups), υC–O–C (stretching of the epoxy group), υC–O (stretching modes of ether and phenolic functionalities), respectively (Acik et al., 2011). The vibrational signatures of hydroxyl, phenols, ethers, carboxylic, and epoxy groups, along with their high intensities, revealed ample oxygen functionalities, making GO a hydrophilic material. The chemical reduction of GO by hydrazine hydrate eliminated most of the oxygen functionalities; thus, vibrational features of oxygen functionalities are diminished significantly (**Figure 4.5b**). The amino groups of ODA showed interaction with epoxide, hydroxyl, and carboxylic functionalities via covalent (nucleophilic substitution reaction), hydrogen–linkages, and charge–induced interactions; as a result, ODA molecules are grafted on GO sheets both within the basal

plane and along the edges (Mungse et al., 2015; Mungse and Khatri, 2014). The appearance of strong peaks in the range of 3000–2800 cm^{-1} was recognized as asymmetric and symmetric stretches of methylene and methyl groups representing the long alkyl chains of ODA grafted on the GO. An intense and broader peak at 1577 cm^{-1} was attributed to an overlapped vibration of N–H linkage along with in–plane stretching of sp^2–hybridized carbon, revealing the confirmation of GO–ODA.

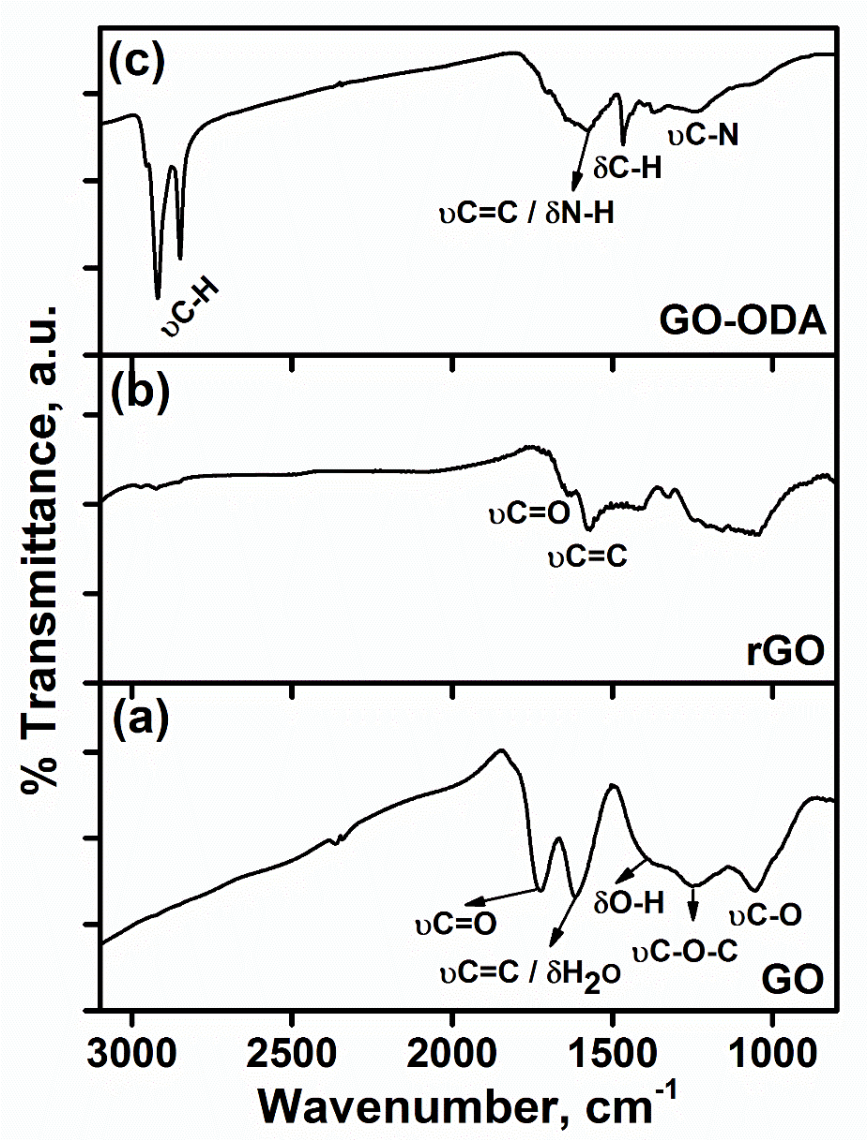

Figure 4.5: FTIR spectra of (a) GO, (b) rGO, and (c) GO–ODA nanosheets along with assignments of vibrational peaks

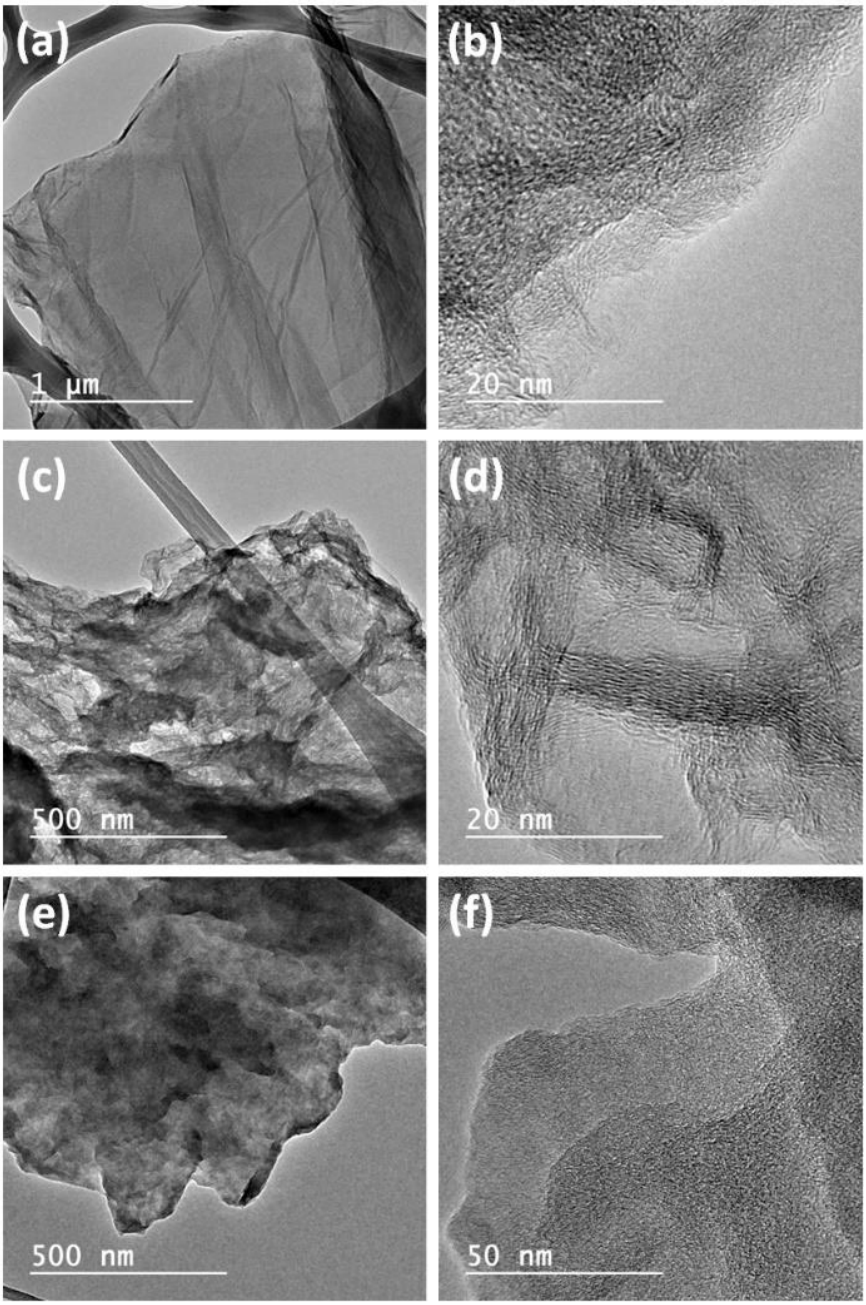

Figure 4.6: TEM images of (a–b) GO, (c–d) rGO, and (e–f) GO–ODA at low and high resolutions

Figure 4.6 shows representative TEM images of GO, rGO, and GO–ODA nanosheets. The microscopic images of GO revealed the crumple and ripple features throughout the sheets. These features are generated because of structural defects and the presence of ample oxygen functionalities in the basal plane of the GO. Higher transparency of GO (**Figure 4.6a**) suggested that GO is composed of a limited number of lamellae. The chemical reduction

of GO made the material (rGO) hydrophobic. The high cohesive interaction between rGO nanosheets makes them pilled–up on each other and furnished the fluffy features, which can be explicitly deduced from **Figure 4.6c**. The high–resolution TEM image (**Figure 4.6d**) of rGO revealed the presence of a limited number of lamellae within an rGO nanosheet along with structural disorders and crumpled features. The lamellar structure with crumpled textures can also be seen in the GO–ODA TEM image (**Figure 4.6e**). However, the degree of crumpled features was decreased to some extent. It might be due to the existence of long alkyl chains in the basal plane, which expanded the interlamellar spacing as revealed from the XRD result (**Figure 4.4**).

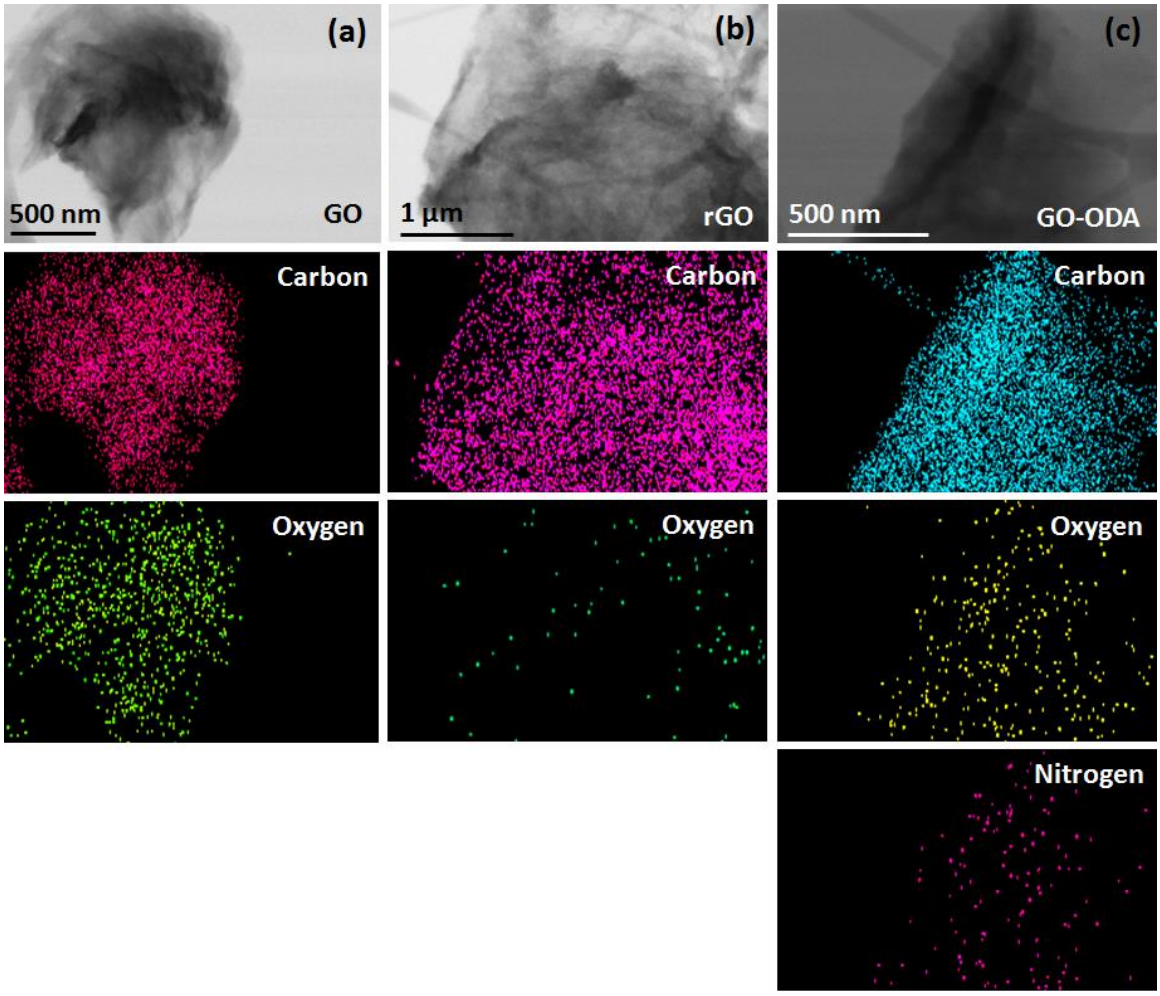

Figure 4.7: Microscopic images of (a) GO, (b) rGO, and (c) GO–ODA along with corresponding area elemental distribution based on EDS measurement

The elemental mapping of graphene–based materials was conducted to probe the existence of characteristics elements. The thorough distribution of oxygen and carbon in the corresponding area of microscopic images (**Figure 4.7a–b**) explicitly revealed that GO and rGO are composed of carbon and oxygen. Furthermore, reduction in oxygen distribution in rGO (**Figure 4.7b**) suggested eliminating of oxygen functionalities to a great extent, which corroborates the FTIR finding. The ODA grafting on GO is deduced from the regular distribution of nitrogen besides the carbon and nitrogen in the GO–ODA (**Figure 4.7c**).

4.3 Physicochemical characterization of paraffin greases

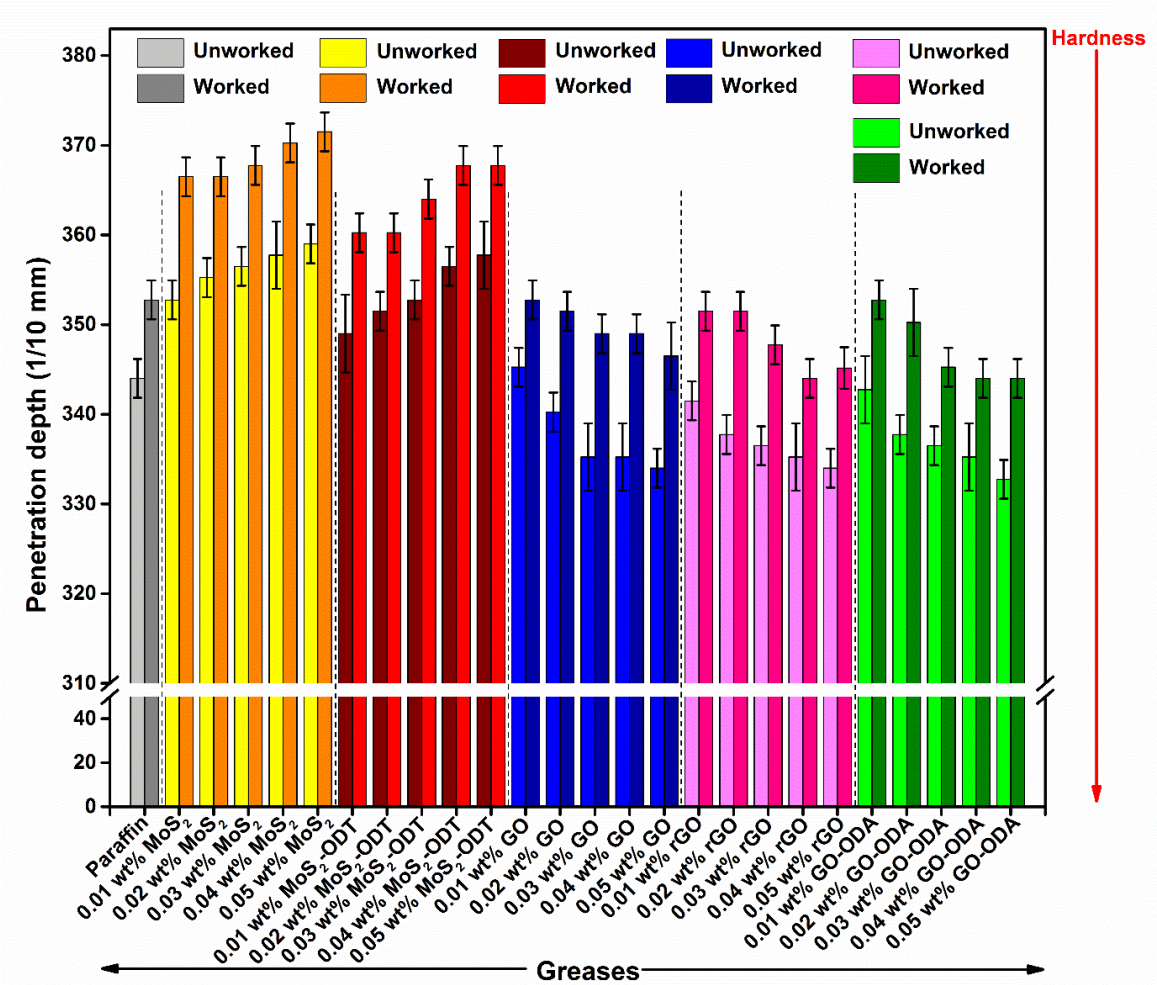

Figure 4.8: Variation in unworked and worked penetration depth of paraffin grease with and without nanoadditives

The paraffin oil–based lithium grease without any nanoadditives is termed as *paraffin grease*. The paraffin grease samples were prepared by blending variable dosages (0.01–0.05 wt%) of MoS_2, MoS_2–ODT, GO, rGO, GO–ODA nanosheets. The paraffin grease thoroughly dispersed with MoS_2, MoS_2–ODT, GO, rGO, and GO–ODA nanosheets is termed as *MoS_2 grease*, *MoS_2–ODT grease*, *GO grease*, *rGO grease*, and *GO–ODA grease*, respectively. Further, paraffin grease was used as a benchmark to compare the physicochemical and tribological properties of paraffin greases with nanoadditives.

The physicochemical properties such as consistency and drop point of grease samples were assessed as per ASTM standards. **Figure 4.8** shows the variation in unworked and worked penetration depths of paraffin grease samples with variable concentrations of nanoadditives. The paraffin grease sample was sheared and examined for the worked penetration depths, indicating the shear stability. After 60 double strokes, the paraffin grease sample showed the NLGI grade 1 consistency.

The MoS_2 and MoS_2–ODT as nanoadditives deteriorated the unworked penetration consistency of paraffin grease. The worked penetration results suggest that the paraffin grease samples blended with MoS_2 and MoS_2–ODT nanoadditives are soft and classified as NLGI 0 grade. The worked penetration depth results also revealed that the grease consistency gradually decreased with increasing doses of MoS_2 and MoS_2–ODT nanoadditives, yet the NLGI grade remained the same. Sometimes, the dispersion of nanoparticles in the grease tends to alter the fibrous structure. Adhvaryu et al. (2005) have revealed that the compactness and cross–linking of the fibrous network of base soap became weak in the presence of additives. Similarly, the addition of α–Al_2O_3 nanoparticles in the commercial lithium grease resulting from the loosening fibrous network of the grease (Singh et al., 2017).

The GO, rGO, and GO–ODA nanoadditives to paraffin grease slightly improved the worked penetration of paraffin grease. However, the worked penetration results suggest that the paraffin grease samples blended with GO, rGO, and GO–ODA nanoadditives are semi–solid and can be classified as NLGI 1 grade. The worked penetration depth results also revealed that the consistency of grease gradually increased with an increasing dose of GO, rGO, and GO–ODA nanoadditives, yet the NLGI grade remained the same. Furthermore, the variation in unworked and worked penetration shows the excellent shear stability of the paraffin with and without nanoadditives.

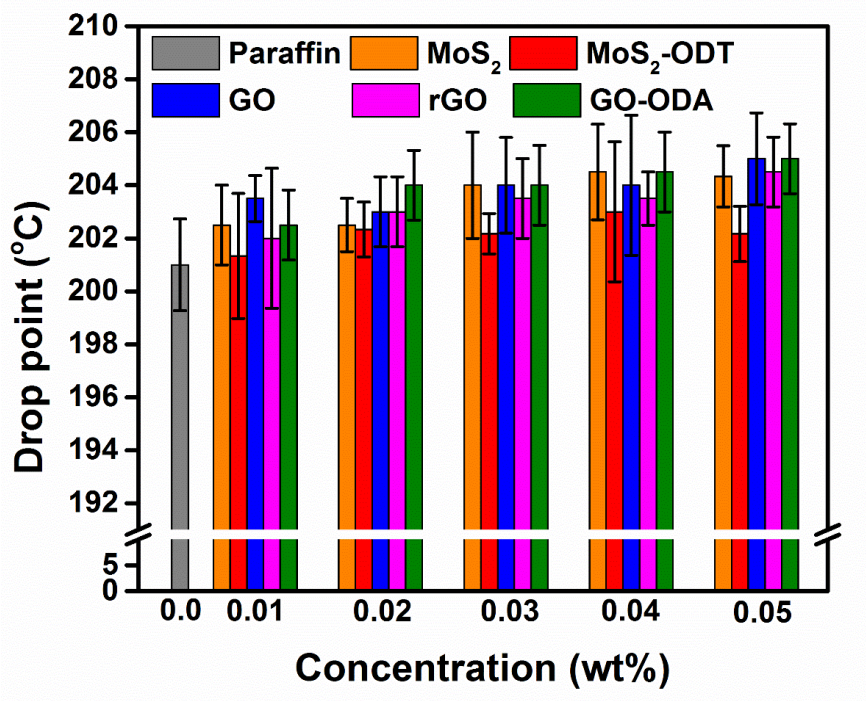

Figure 4.9: Variation in drop point of paraffin grease with and without nanoadditives

The drop point is dependent on the type of thickener used in the formulation of the grease. It is a critical property to evaluate the performance of the grease. When the grease is heated, it softens and turns its phase from semi–solid to liquid. This test indicates the temperature at which the thickener cannot hold the base oil in its matrix. **Figure 4.9** shows the variation in drop point of paraffin grease with variable concentrations of nanoadditives. The drop

point of paraffin grease was not improved significantly with the addition of nanoadditives. It showed only 4 °C increment of temperature with 0.05 wt% of the nanoadditives.

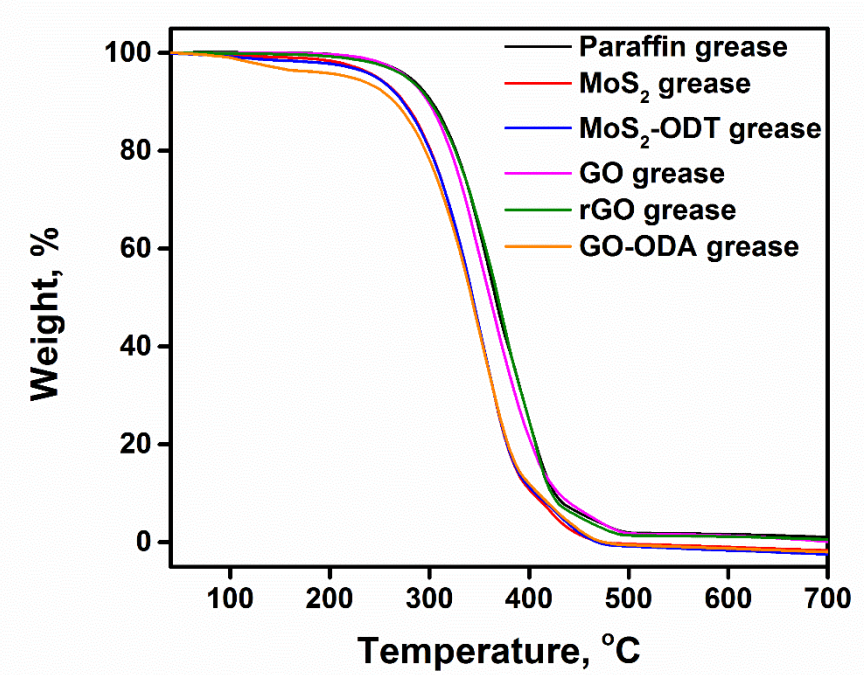

Figure 4.10: Thermal degradation patterns of paraffin grease with and without nanoadditives

Figure 4.10 shows a thermal degradation of paraffin grease and its blended with MoS_2, MoS_2–ODT, GO, rGO, and GO–ODA nanosheets. All grease samples displayed single–step thermal degradation, revealing the homogeneous chemical structure of paraffin grease (Sánchez et al., 2011). The onset temperature was determined from the interception between the slope of the weight loss and the region, where the weight is almost constant. The high onset temperature (T_{onset} =300 °C) indicated excellent thermal stability of paraffin grease. The maximum thermal decomposition (T_{max}) occurred at 380 °C. The T_{onset} and T_{max} of MoS_2 and MoS_2–ODT, GO, rGO, and GO–ODA nanosheets doped greases are summarized in **Table 4.1**. The paraffin grease blended with MoS_2 and MoS_2–ODT, GO, rGO, and GO–ODA nanosheets showed T_{onset} having almost similar values to paraffin grease, signifying excellent thermal stability of all grease samples. Further, no significant

weight loss was observed at a lower temperature (50–120 °C), and it rules out the presence of water in the grease. The drop points of the MoS_2 and MoS_2–ODT, GO, rGO, and GO–ODA nanosheets doped paraffin greases were observed in the range of 201–205 °C, which is significantly lower than their T_{onset} and T_{max} temperatures.

Table 4.1: Thermogravimetric analysis of various paraffin oil–based greases

Samples	Onset temperature (T_{onset}), °C	Maximum decomposition temperature (T_{max}), °C
Paraffin grease	300	380
MoS_2 grease	292	351
MoS_2–ODT grease	291	351
GO grease	304	360
rGO grease	305	375
GO–ODA grease	290	379

4.4 Tribological performance of paraffin greases on four–ball tester

The frictional behavior of paraffin grease with and without doping of MoS_2, MoS_2–ODT, GO, rGO, and GO–ODA nanosheets were evaluated using the four–ball tester as per the ASTM D2266 standard. **Figure 4.11** shows changes in the average COF with increasing doses of MoS_2, MoS_2–ODT, GO, rGO, and GO–ODA nanosheets in the paraffin grease. The pristine paraffin grease displays the high COF ($\mu = 0.094$) of the mating surfaces (i.e., steel balls) under the sliding contact at a load of 392 N. The doping of MoS_2, MoS_2–ODT, GO, rGO, and GO–ODA nanosheets decreased the COF, variable with their dosage in the paraffin grease. The 0.04 and 0.01 wt% doses of MoS_2 and MoS_2–ODT nanosheets in paraffin grease exhibited a reduction in COF ~42% in both cases.

The GO and rGO greases exhibited minimum friction at their blending of 0.01 wt%, which are 34% and 50% lower than that of paraffin grease, respectively. The GO–ODA grease

showed a maximum reduction in friction (~34%) at blending of 0.05 wt%. The high–resolution TEM image of rGO (**Figure 4.6d**) exhibited a limited number of stacked lamellae. The reduction of oxygen functionalities and the restoration of sp^2 carbon in the rGO provide low interfacial shear strength, decreasing the frictional force. Among all samples, rGO–doped grease showed minimum friction. It attributes the low shear properties of rGO because of the weak van der Waals interaction between their adjacent atomic lamellae having an interlamellar spacing of 0.35 nm.

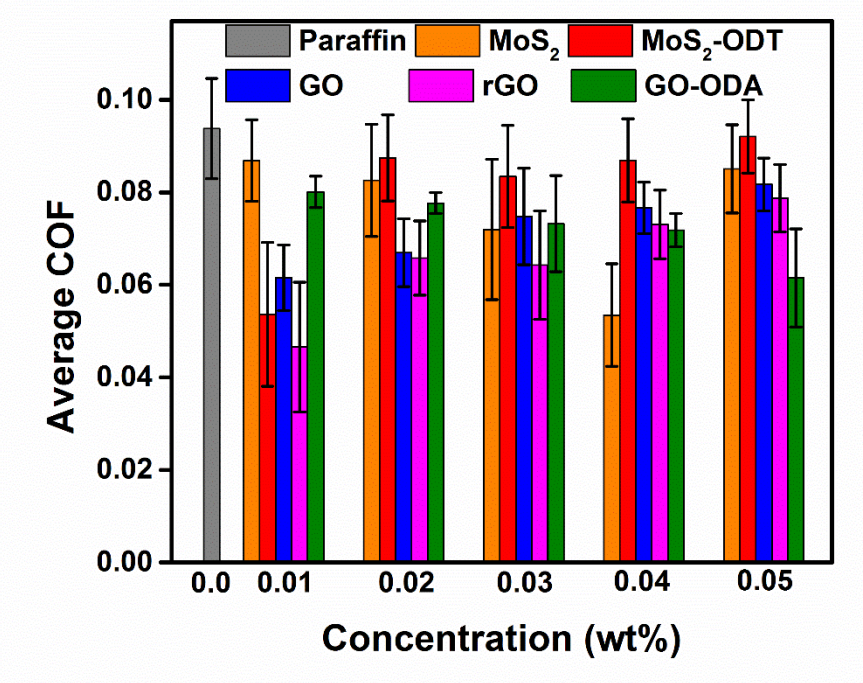

Figure 4.11: Variation in average COF with variable concentration of nanoadditives blended with paraffin grease. (Applied load: 392 N, test duration: 60 min)

Figure 4.12 shows the variation in coefficient of friction (COF) as a function of time for paraffin grease and its blend with MoS_2 (0.04 wt%) and MoS_2–ODT (0.01 wt%), GO (0.01 wt%), rGO (0.01 wt%), and GO–ODA (0.05 wt%) nanosheets. The paraffin grease exhibited a higher COF throughout the running–in period. The presence of several undulations in the friction profile indicated that paraffin grease is unable to maintain the continuous tribo–film on the steel balls. It could also be happening by entrapping wear

debris generated during the frictional contact (Gupta and Harsha, 2018a). Doping of MoS_2 and MoS_2–ODT nanosheets significantly decreased the COF. Such reduction was higher during the initial period of rotational contact, signifying that MoS_2 establishes a better tribo–film between the contacting surfaces. The reductions of undulations in friction profiles of MoS_2 and MoS_2–ODT–doped greases further revealed the formation of a comparatively good quality of the tribo–film, which avoided the direct contact of the steel balls and furnished a low and relatively stable friction profile.

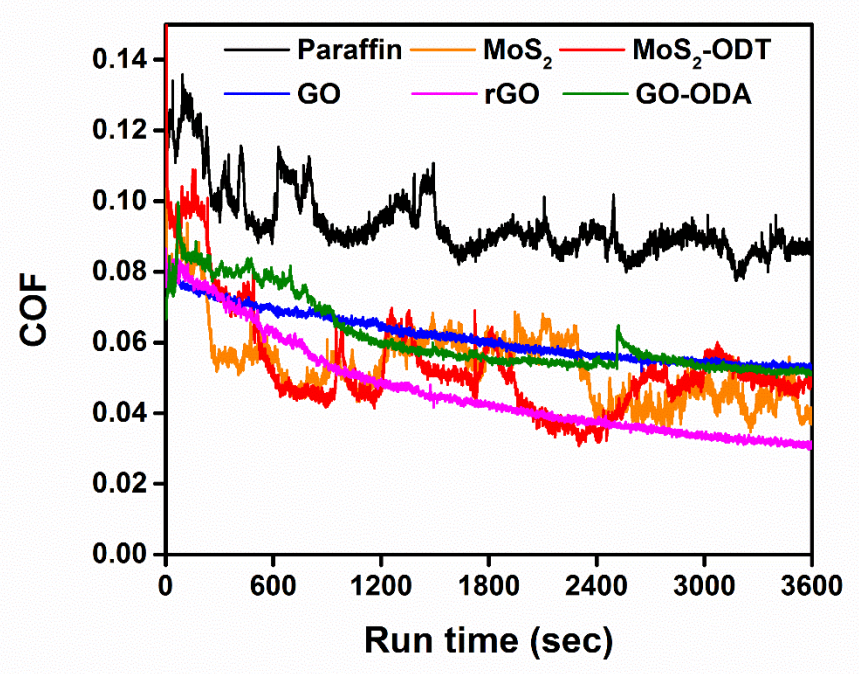

Figure 4.12: Variation in COF with time for paraffin grease and its blend with nanoadditives. (Applied load: 392 N, test duration: 60 min)

The smooth and stable friction profiles of GO, rGO, and GO–ODA greases indicate a continuous supply of graphene oxide–based nanomaterial at the rubbing surfaces. The continuous supply of additives maintains a stable tribo–film between tribo–pairs. The formation of graphene–based tribo–film decreased the friction by providing low shear properties and avoided the direct interaction between the tribo–interfaces. Therefore, graphene–based materials as nanoadditives furnished a low and stable friction profile,

unlike paraffin grease. Choudhary et al. (2012) have revealed that the uninterrupted supply of graphene on the tribo–interfaces is very important to enhancing lubricity

Table 4.2: Energy saving with the use of MoS_2, MoS_2–ODT, GO, rGO, and GO–ODA nanoadditives in paraffin grease

Samples	Parameters	Concentration (wt%)					
		0.0	**0.01**	**0.02**	**0.03**	**0.04**	**0.05**
MoS_2 grease	Power consumption (MJ)	74.6	69.1	65.7	57.3	42.5	67.7
	% reduction in power consumption	—	7	12	23	43	9
MoS_2–ODT grease	Power consumption (MJ)	74.6	42.7	69.6	66.4	69.2	73.3
	% reduction in power consumption	—	43	7	11	7	2
GO grease	Power consumption (MJ)	74.6	49.0	53.3	59.5	61.0	65.0
	% reduction in power consumption	—	34	29	20	18	13
rGO grease	Power consumption (MJ)	74.6	37.0	52.4	51.1	58.1	62.6
	% reduction in power consumption	—	50	30	31	22	16
GO–ODA grease	Power consumption (MJ)	74.6	63.7	61.8	58.3	57.1	48.9
	% reduction in power consumption	—	15	17	22	23	34

The friction represents a wastage of energy in the form of heat during the tribo–tests. The energy consumed during tribo–tests using the paraffin grease samples, having a variable dosage of MoS_2, MoS_2–ODT, GO, rGO, and GO–ODA nanosheets, are summarized in **Table 4.2**. The paraffin grease consumed maximum energy (74.6 MJ) to overcome the frictional losses. The presence of nanoadditives conserves the energy by reducing frictional losses. The optimized dosage of MoS_2, MoS_2–ODT, GO, rGO, and GO–ODA saved energy by ~43%, ~43%, ~34%, ~50%, and ~34%, respectively. These results suggest that the

incorporation of minute dosage of nanoadditives has significant potential to conserve the energy.

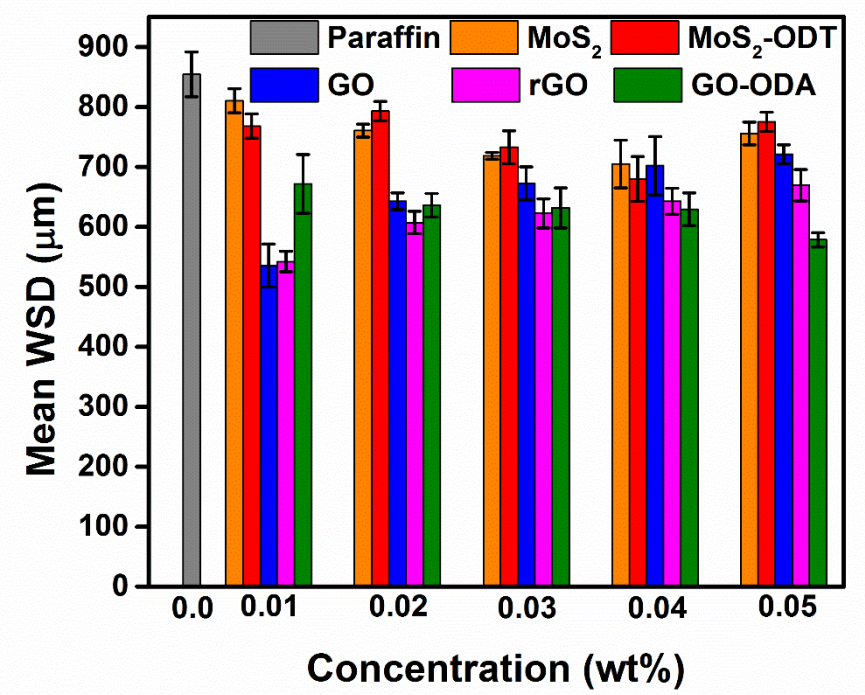

Figure 4.13: Variation in mean WSD with variable concentration of nanoadditives blended with in paraffin grease. (Applied load: 392 N, test duration: 60 min)

Figure 4.13 displays the change in wear scar diameter (WSD) for grease samples with variable dosages (0.01 to 0.05 wt%) of MoS_2, MoS_2–ODT, GO, rGO, and GO–ODA nanosheets. The paraffin grease has developed a more prominent wear scar (ϕ = 854 μm) on the steel balls. The presence of MoS_2 and MoS_2–ODT nanosheets has reduced the WSD with variable doses of MoS_2 and MoS_2–ODT nanosheets. The 0.04 wt% dose of MoS_2 and MoS_2–ODT nanosheets showed a maximum reduction in WSD and was found to be 17% and 20%, respectively. The 0.01 wt% of GO and rGO nanosheets as an additive to paraffin grease decreased the WSD by (~37%), while 0.05 wt% of GO–ODA showed maximum reduction (~32%) in the WSD. The significant decrease in WSD by dispersion of MoS_2, MoS_2–ODT, GO, rGO, and GO–ODA nanosheets in the grease qualified them as excellent antiwear nanoadditives.

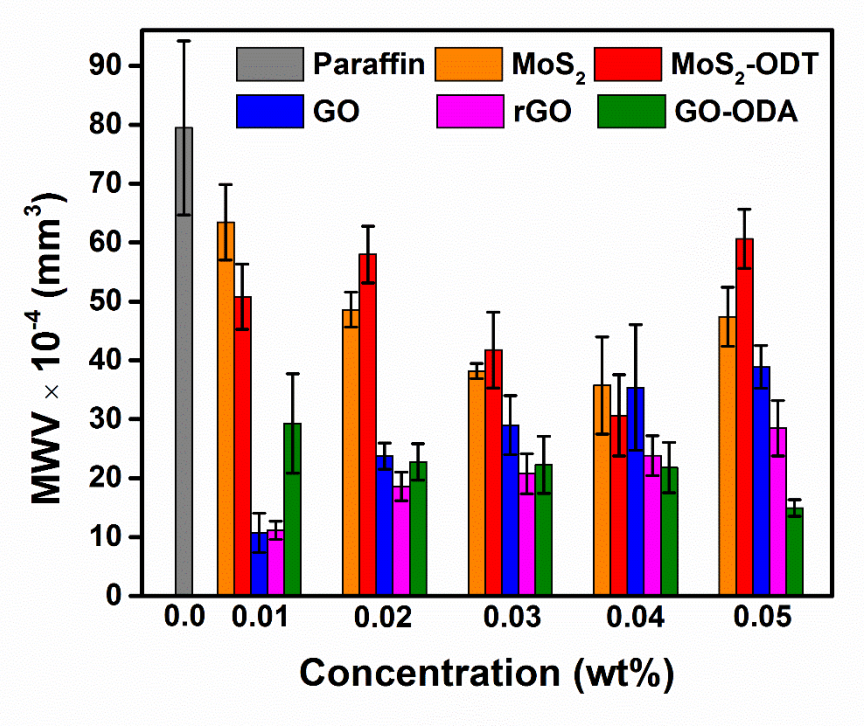

Figure 4.14: Variation in MWV of steel balls lubricated with paraffin grease and its blend with variable concentration of nanoadditives. (Applied load: 392 N, test duration: 60 min)

Figure 4.14 shows the changes in mean wear volume (MWV) for grease samples having a variable concentration of MoS_2, MoS_2–ODT, GO, rGO, and GO–ODA nanosheets. The 0.04 wt% of MoS_2 nanosheets exhibited maximum reductions in MWV (~55%), whereas 0.04 wt% of MoS_2–ODT showed maximum reduction in MWV (61%) compared to the paraffin grease. The 0.01 wt% of GO and rGO as an optimized dose furnished maximum reduction (~86%), whereas 0.05 wt% of GO–ODA exhibited maximum decrease (~81%) in the MWV. The paraffin grease showed the highest COF, WSD, and MWV among all grease samples being studied. These results revealed the lubricious properties of MoS_2, MoS_2–ODT, GO, rGO, and GO–ODA nanoadditives in paraffin grease to lower and stabilize the friction by the formation of tribo–film on` interacting surfaces but also protecting the tribo–bodies by reducing the WSD and MWV.

4.5 Microstructural properties of the paraffin grease

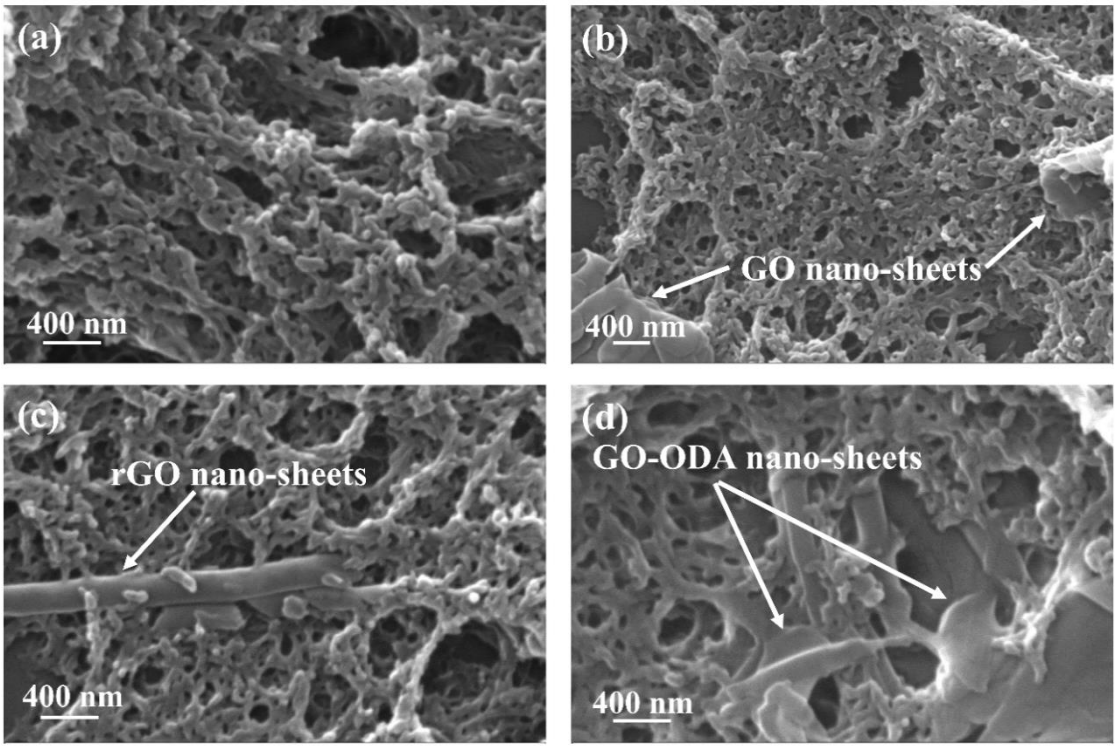

Figure 4.15: SEM micrographs of (a) paraffin (b) GO (c) rGO, and (d) GO–ODA greases after extraction of oil

Figure 4.15 depicts representative micrographs of grease samples after extracting the paraffin oil. The fibrous structure made by lithium soap thickener can be explicitly seen in all samples. Various physiochemical properties of grease were influenced by the structure and nature of the thickener (Fan et al., 2018). The fibrous network of thickeners yielded the voids throughout the samples. The lube base oil is trapped in these voids driven by capillary and van der Waals interactions (Lugt, 2009). The presence of GO, rGO, and GO–ODA in the fibrous grease network is indicated by white arrows (**Figure 4.15b–d**). The graphene–based nanosheets maintained the fibrous structure of grease significantly, which is very important for viscoelastic properties. However, it is observed that void size, particularly around the graphene–based sheets, is increased. Adhvaryu et al. (2005) have reported that a more significant and looser network structure of the soap in association with

nanoadditives. The looser fiber network of soap in the presence of graphene–based additives allow the release of more base oil and additives at the tribo–interfaces and lubricates them efficiently. Under the tribo–stress, the paraffin oil and graphene–based sheets trapped in the fibrous structure are squeezed out and lubricate the sliding surfaces. The lube base oil, additives, and thickener of grease collectively contribute to the development of tribo–film to enhance tribological properties (Fan et al., 2018).

4.6 Rheological behavior of grease

Figure 4.16 illustrates that paraffin grease shear stress is considerably higher than the GO, rGO, and GO–ODA greases throughout the range of shear strain. It was observed that thoroughly blended graphene–based nanoadditives decreased the shear stress of paraffin grease. The doping of graphene–based materials increased the void area and compromised the compactness of the fibrous structure. As a result, trapped paraffin oil and graphene–based sheets are quickly discharged from the grease matrix when the small shear stress is applied. Adhvaryu et al. (2005) have revealed that the compactness and cross–linking of the fibrous network of base soap became weak in the presence of additives. The loosing of a cross–linked network of thickener by graphene–based nanoadditives facilitates the discharge of trapped oil under the tribo–stress to lubricate the surfaces and forms the tribo–film, graphene–based nanoadditives play a vital role in the enhancement of tribological properties. The low and stable friction profiles of GO, rGO, and GO–ODA greases affirmed the formation of a better tribo–film than paraffin grease, where both microstructural features of grease and the presence of graphene–based additive collectively improved the tribological properties (**Figure 4.11**–**Figure 4.14**). The shear stress–strain results of all samples were fitted with a Herschel–Bulkley rheological model and extracted yield stress, shear–thinning index, consistency factor, and correlation coefficient, which are shown in

Table 4.3. The high correlation coefficient confirmed an excellent fitting of experimental results to the Herschel–Bulkley model. The performance of grease samples based on yield stress under the shear was found in the order of paraffin grease > GO–ODA grease > rGO grease > GO grease.

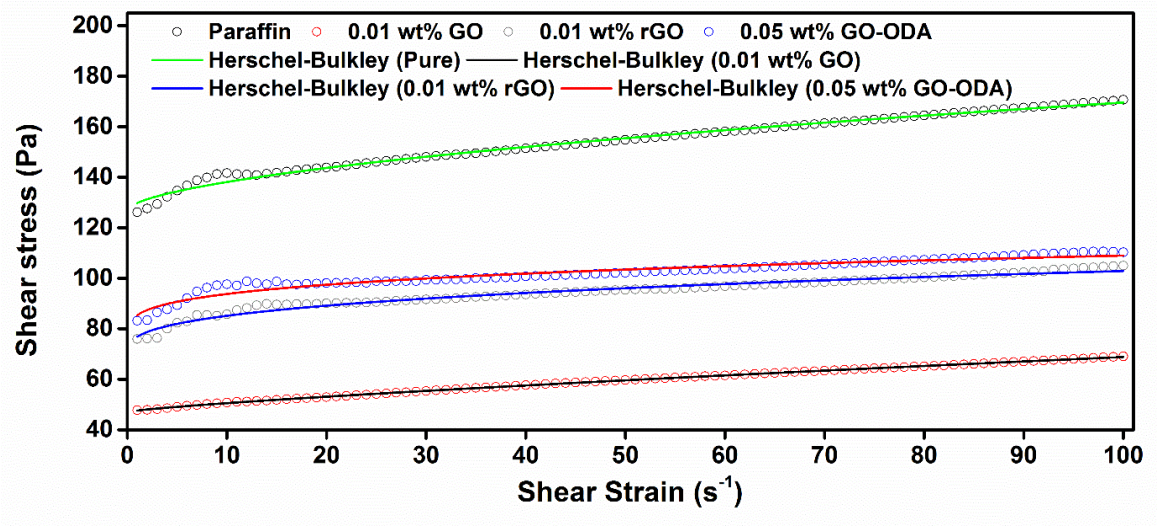

Figure 4.16: Shear stress vs. shear strain curve for paraffin, GO, rGO, and GO–ODA greases along with fitting of experimental results as per the Herschel–Bulkley model

Table 4.3: Rheological parameters calculated through the Herschel–Bulkley model by fitting the experimental results of shear stress vs. strain for paraffin, GO, rGO, and GO–ODA greases

Parameters	Paraffin grease	GO grease (0.01 wt%)	rGO grease (0.01 wt%)	GO–ODA grease (0.05 wt%)
Temperature, ^{o}C	75	75	75	75
τ_y, Pa	126.84	47.07	69.52	75.01
k, Pa.s^n	2.97	0.55	7.30	10.36
n	0.58	0.80	0.33	0.26
R	0.99	0.99	0.97	0.93

Figure 4.17 displays the variation in the apparent viscosity of paraffin, GO, rGO, and GO–ODA greases as a function of shear strain. The GO, rGO, and GO–ODA greases exhibited

lower viscosity than paraffin grease at low shear strain, indicating the fibrous structure of grease. It is modified by thoroughly dispersed graphene–based nanosheets, making paraffin oil availability easier even at low shear strain and viscosity decreased than paraffin grease. The viscosity of all samples sharply decreased with increasing shear strain, and it suggested the thixotropic behavior of grease samples. No significant change in viscosity is observed at high shear strain, indicating that thoroughly dispersed graphene–based nanoadditives do not affect viscosity at a high shear strain.

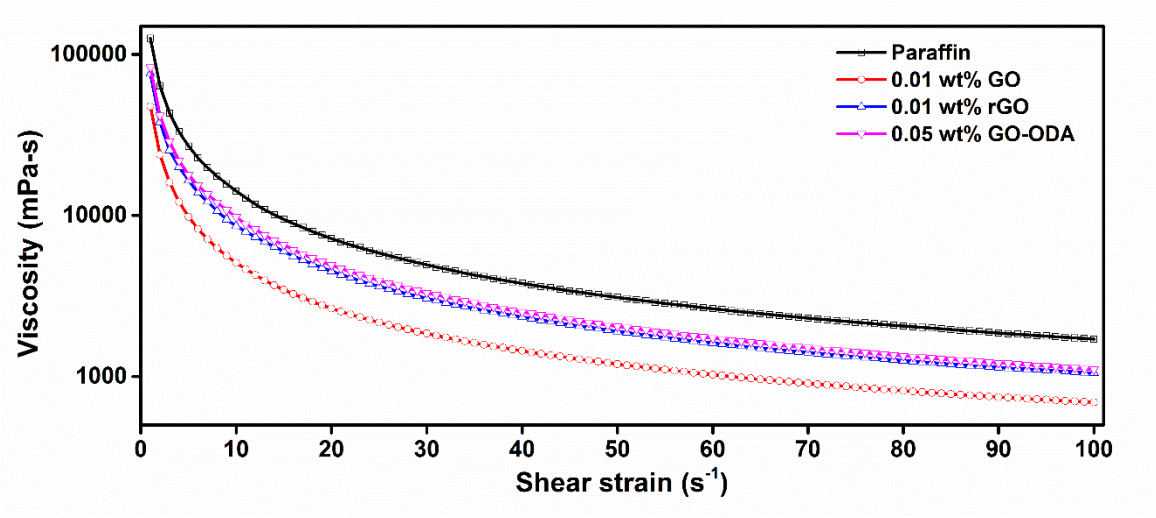

Figure 4.17: Viscosity of paraffin, GO, rGO, and GO–ODA greases as a function of shear strain

The storage modulus (G') is a quantitative measurement of stiffness at low strain. The stiffness of the grease spells the interaction between the grease components, i.e., soap, base oil, and additives. **Figure 4.18** shows the variation of storage and loss modulus (G") in the angular frequency range of 0–100 rad/s for the paraffin and GO, rGO, GO–ODA greases. The storage moduli of all samples were significantly higher than the loss moduli within the whole frequency range. After the initial running–in period, the G' and G" were independent of the angular speed. The storage modulus influences the tribological performance of the grease. The grease with a low storage modulus shows excellent potential to form a tribo–

film compared to the greases having high storage modulus (Couronné et al., 2003). The paraffin grease with a high storage modulus exhibited higher wear and friction, attributed to the poor tendency to form a lubricious thin film. The higher storage modulus made paraffin grease ineffective in releasing a sufficient amount of base oil to lubricate the rubbing surfaces compared to graphene–based greases. The absence of undulations in friction profiles of GO, rGO, and GO–ODA greases (**Figure 4.12**) further corroborate the development of a sustainable tribo–film.

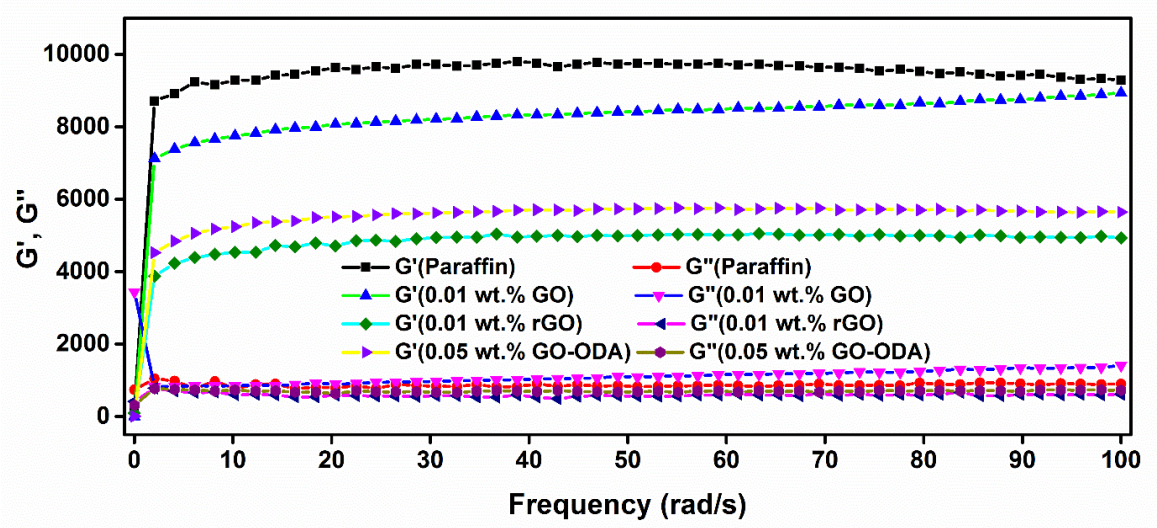

Figure 4.18: Storage and loss modulus of paraffin, GO, rGO, and GO–ODA greases

4.7 Study of worn surfaces tested on four–ball tester

Figure 4.19a displays the SEM micrographs of worn surface of steel ball lubricated with paraffin grease. It exhibited deep furrows and scratches marks, revealing the severity of wear and material loss. As can be easily seen in the high–resolution micrographs (**Figure 4.19b**), the wear pattern illustrates the adhesive wear because of poor film formation, which is further supported by the presence of undulation in the friction profile.

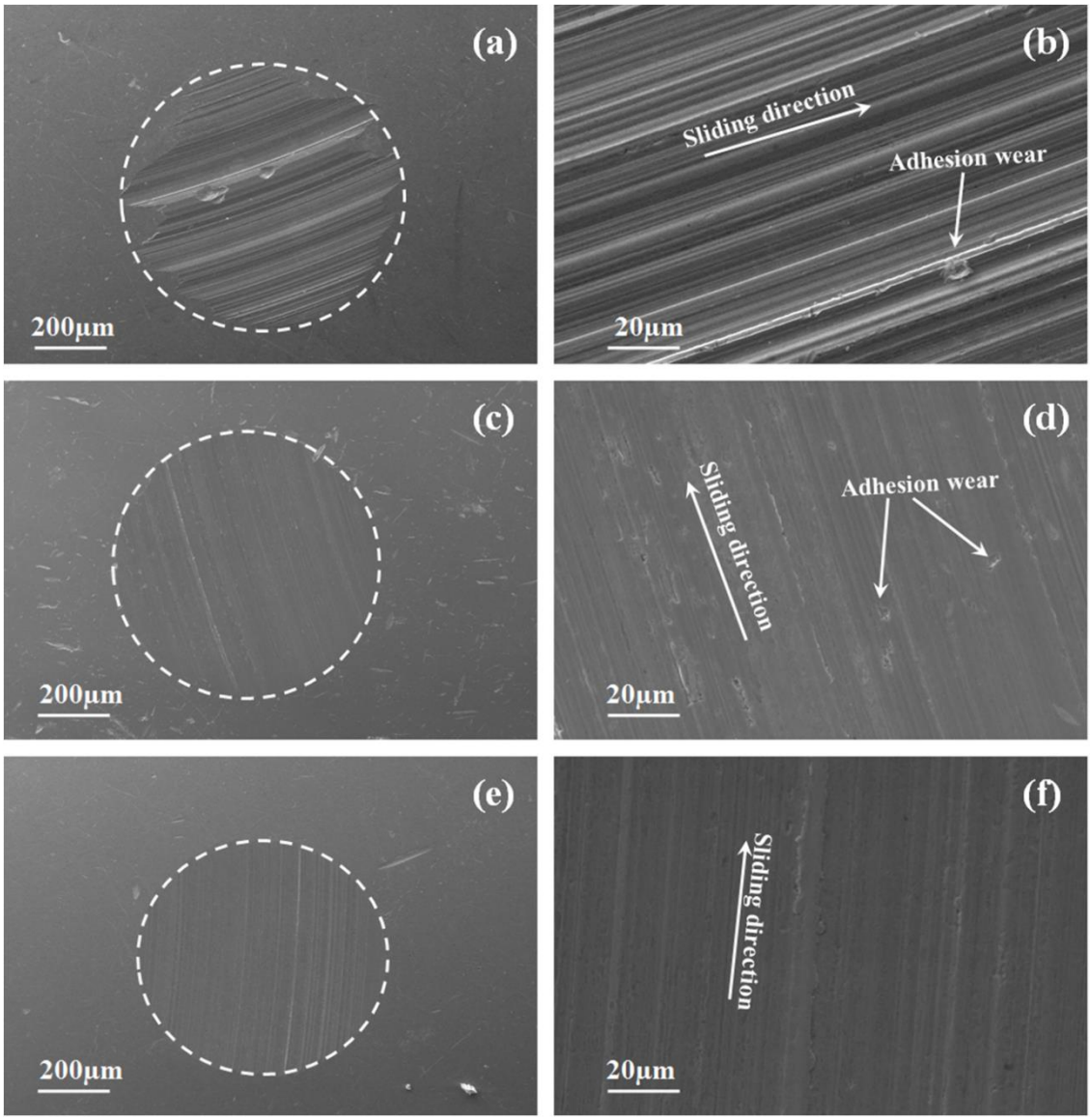

Figure 4.19: SEM images of worn surfaces of steel balls lubricated with (a–b) paraffin grease, (c–d) 0.04 wt% MoS_2 blended grease (e,f) 0.04 wt% MoS_2–ODT blended grease. (Applied load: 392 N, test duration: 60 min)

The paraffin grease having 0.04 wt% of MoS_2 and MoS_2–ODT nanosheets significantly reduced the severity of wear by subsiding the scratches and furrows on the worn surfaces (**Figure 4.19c–f).** It is further supported by a reduction in wear volume **(Figure 4.14).** The worn surfaces were smoothened in the presence of MoS_2 and MoS_2–ODT blended greases compared to paraffin grease, which suggested that MoS_2 as an additive plays a vital role in protecting the contact surfaces against wear. Furthermore, the dangling sulfur atoms in the outer layer of functionalized MoS_2 nanosheets plausible played a role in reducing the wear.

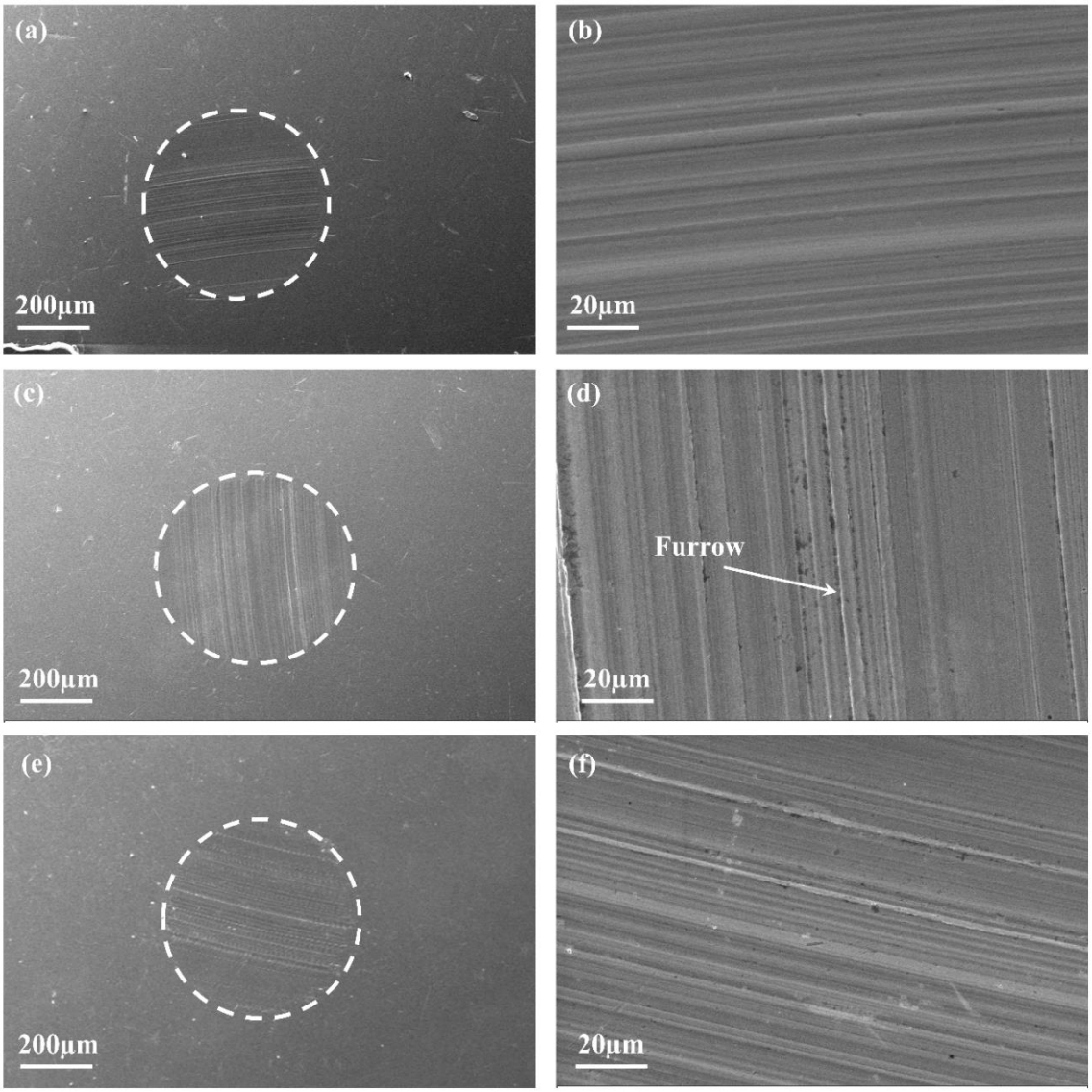

Figure 4.20: SEM images of worn surfaces of steel balls lubricated with (a–b) 0.01 wt% GO blended grease (c–d) 0.01 wt% rGO blended grease (e–f) 0.05 wt% GO–ODA blended grease. (Applied load: 392 N, test duration: 60 min)

Figure 4.20 shows the micrographs of worn steel balls lubricated by GO, rGO, and GO–ODA greases. The presence of graphene–based nanoadditives in grease has significantly reduced the magnitude of wear scar and severity of plastic damage (**Figure 4.20a–f**). The point contact geometry of four balls under the tribo–stress yielded the Hertzian contact stress of ~3.4 GPa. The heat generation at the interfaces because of friction and high stress leads to the softening of the grease. The high contact stress and softening of the grease have led to the release of thoroughly dispersed graphene–based nanoadditives. It has lubricated

the contact interfaces by forming a thin boundary film, which protected the tribo–pair by reducing the wear. The lube oil and thickener also contributed to creating a protective tribo–film (Stachowiak and Batchelor, 2013). The soap molecules and graphene–based nanoadditives on the contact interfaces were easily sheared by high tribo–stress, and decreased friction. A protective film was developed through the adsorption of graphene–based nanoadditives on the worn surfaces (Fan et al., 2014; Gan et al., 2020). This film reduces the direct contact of asperities and improves surface roughness, antiwear (AW), and antifriction (AF) properties.

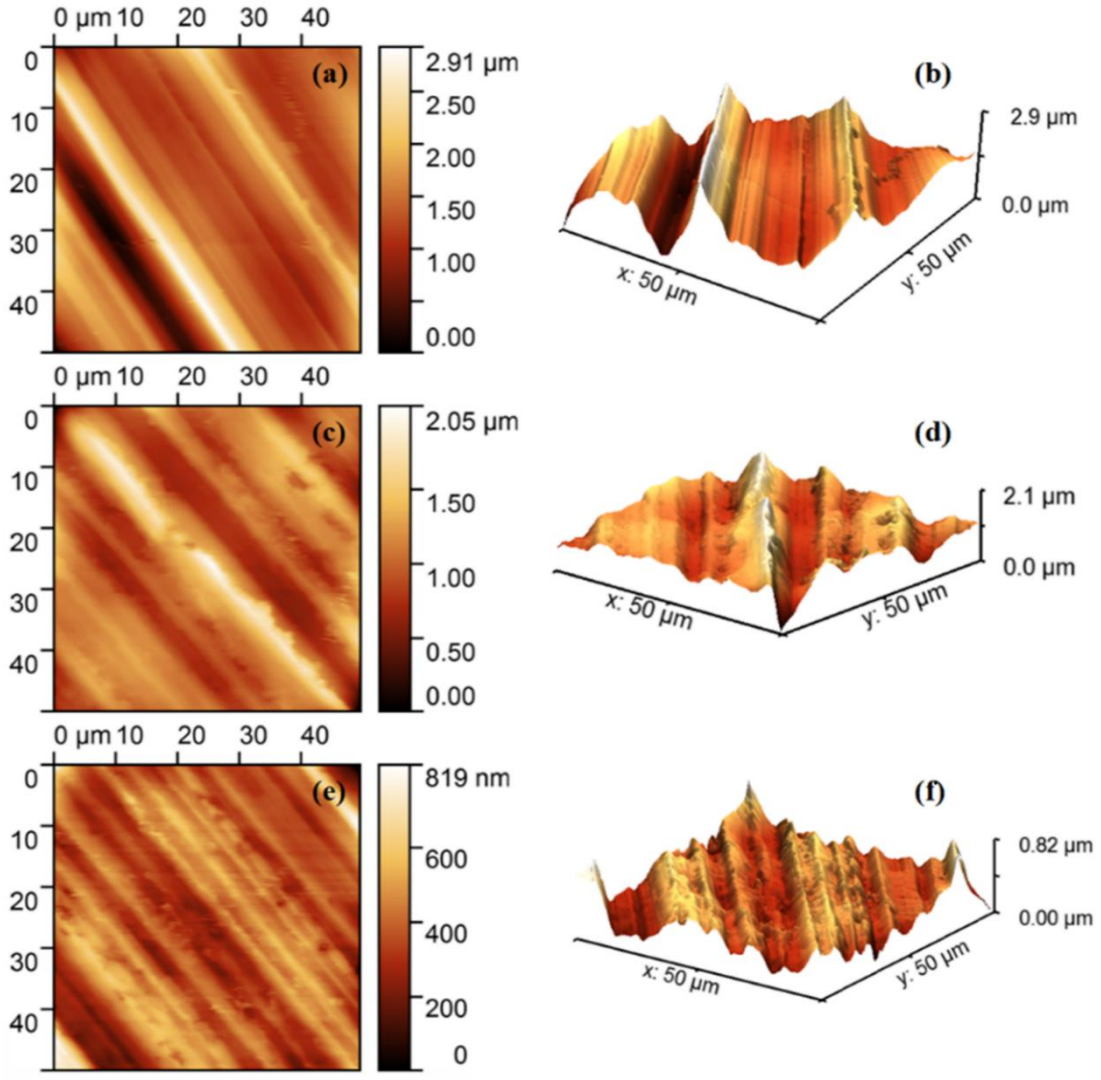

Figure 4.21: Topographic images of the worn surfaces of steel balls lubricated with (a–b) paraffin grease, (c–d) 0.04 wt% MoS_2 blended grease (e,f) 0.04 wt% MoS_2–ODT blended grease (Applied load: 392 N, test duration: 60 min)

The topographic image of worn surface of steel ball lubricated with paraffin grease was collected by SPM to quantify the roughness features. The topographic image and corresponding three-dimensional (3D) view (**Figure 4.21a–b**) of the steel ball explicitly illustrate many deep scratches and furrows with sharp edges, indicating the severity of wear of steel balls in the sliding direction. As a result, very high roughness was observed. The 3D image revealed the severity of wear in the form of the high stick–slip events supported by corrugated features because of high adhesion–driven wear. It further corroborates the friction and wear results that paraffin grease could not form a good quality tribo–film. The several undulations in the friction profile of paraffin grease (**Figure 4.12**) confirmed the poor–quality thin film along with the possibility of intermittent contact between the steel balls. The local coalescence of asperities and then breaking adhesive junctions due to sliding removed the materials in the form of wear (**Figure 4.21b**). The adhesive wear features are also explicitly seen in the SEM image (**Figure 4.19b**).

Table 4.4: Roughness of worn surfaces of the steel balls lubricated with various paraffin greases

Samples	Line roughness		Surface roughness	
	Ra, nm	Rq, nm	Sa, nm	Sq, nm
Paraffin grease	1070	1220	987	1190
MoS_2 grease	275	336	308	385
MoS_2–ODT grease	99	129	104	132
GO grease	42	52	94	117
rGO grease	35	48	54	70
GO–ODA grease	41	56	206	252

The doping of 0.04 wt% MoS_2 or MoS_2–ODT in the paraffin grease has decreased the roughness and yielded comparatively smoother surface features (**Figure 4.21c–f**). The linear roughness measured in the transverse to sliding direction and surface roughness of

worn areas lubricated with various grease samples based on SPM measurements is presented in **Table 4.4**. The surface roughness (1190 nm) of steel ball lubricated with paraffin grease reduced by ~67% and ~89% in the presence of 0.04 wt% MoS_2 or MoS_2–ODT nanosheets, respectively. The reduction in the roughness of worn surfaces by MoS_2 nanosheets revealed their function in establishing a tribo–film between the mating surfaces.

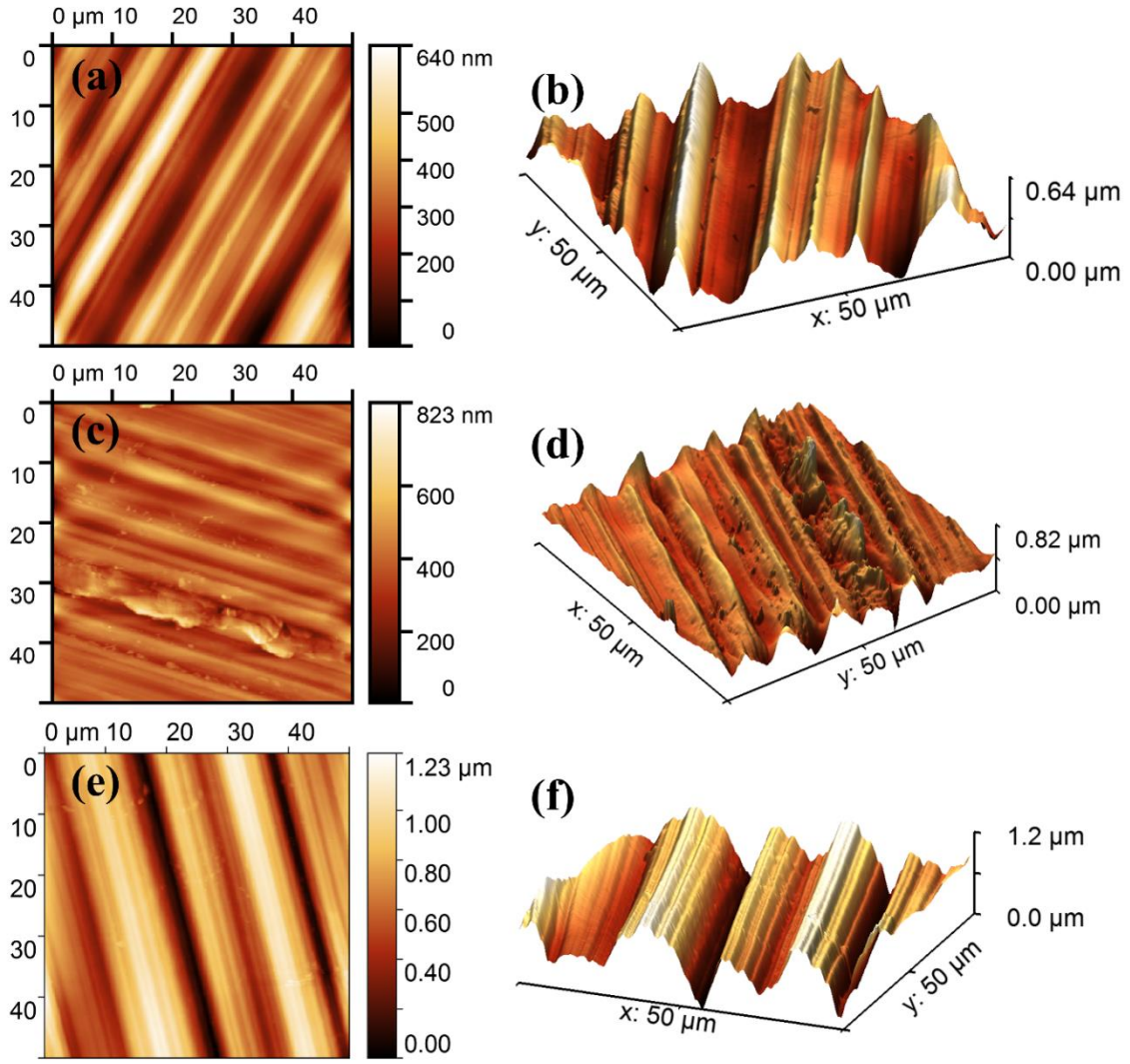

Figure 4.22: Topographic images of the worn surfaces of steel balls lubricated with (a–b) 0.01 wt% GO blended grease, (c–d) 0.01 wt% rGO blended grease (e–f) 0.05 wt% GO–ODA blended grease. (Applied load: 392 N, test duration: 60 min)

The steel balls lubricated with GO, rGO, and GO–ODA greases showed significantly lower peak–to–peak roughness than paraffin grease (**Figure 4.22a–f**). Furthermore, adhesive

wear features vanished because of graphene–based nanoadditives, preventing the direct interaction between the steel balls. In the presence of 0.01 wt% GO, and 0.01 wt% rGO, and 0.05 wt% GO–ODA nanosheets, the surface roughness of steel balls lubricated with paraffin grease was reduced by ~90%, ~94%, and ~79%, respectively. Among all samples, steel ball lubricated with rGO grease showed the lowest roughness indicating significant improvement in AW properties.

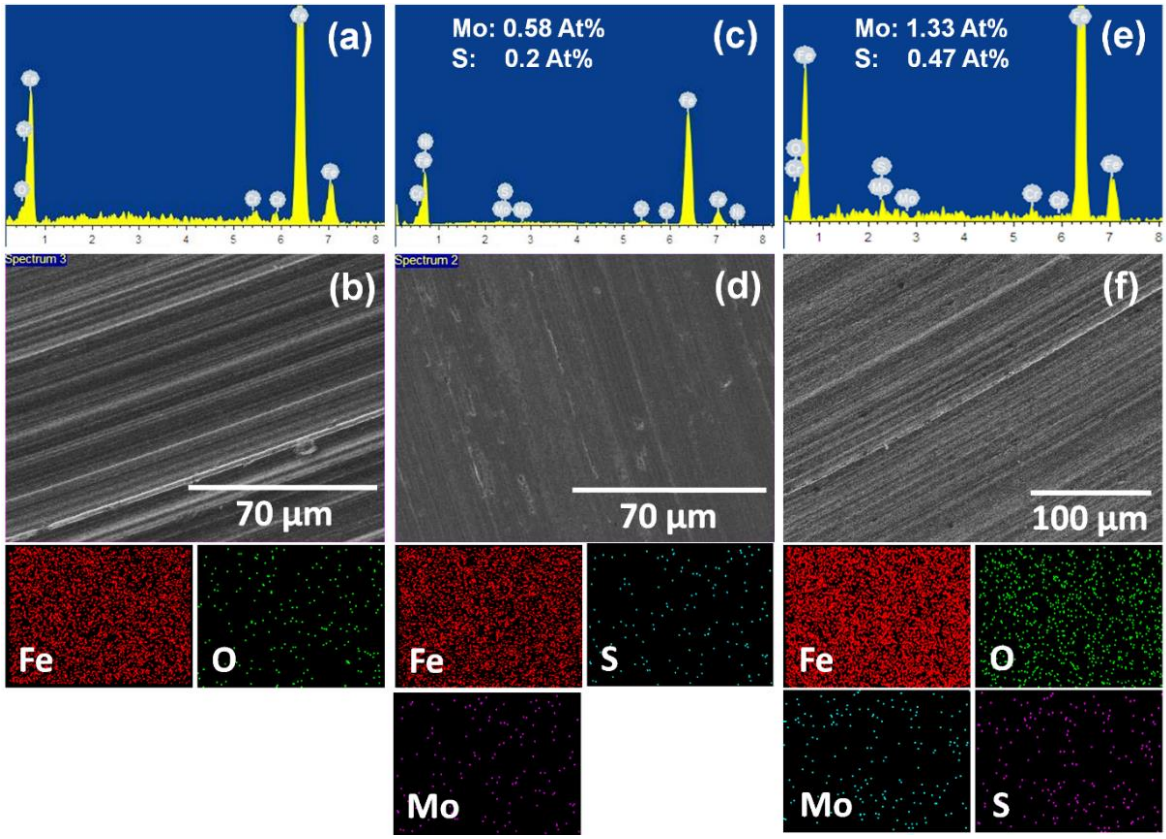

Figure 4.23: EDS spectra with elemental mapping of worn surfaces of steel balls lubricated with (a–b) paraffin grease (c–d) 0.04 wt% MoS_2 blended grease (e–f) 0.04 wt% MoS_2–ODT blended grease. (Applied load: 392 N, test duration: 60 min)

The EDS spectra and elemental distribution images of worn surfaces were collected to probe the chemical nature and participation of MoS_2, MoS_2–ODT, GO, rGO, and GO–ODA nanosheets establishment of boundary tribo–film on the mating interfaces of steel balls. **Figure 4.23a,c,e** shows EDS spectra of steel balls lubricated with paraffin grease, MoS_2

and MoS_2–ODT–doped paraffin greases, along with the at% of the individual elements on worn surfaces. Simultaneously, the elemental mapping of the selected worn area of each sample was executed to examine the elemental distribution in the established tribo–film. **Figure 4.23a** shows the EDS spectrum of worn surface lubricated with paraffin grease. The worn surface lubricated with paraffin grease showed an intense and uniform distribution of iron and alloying elements of steel rules out the presence of foreign particles or additives. The presence of oxygen was ascribed to the oxidation of the worn surface of steel balls. The steel balls lubricated with MoS_2 and with MoS_2–ODT–blended grease samples exhibited the uniform distribution of Mo and S beside the core elements of steel balls, which confirmed the deposition of MoS_2–based materials on the mating interfaces.

Figure 4.24a–b shows the EDS spectra and the elemental distribution characteristics of worn steel balls lubricated with GO and rGO greases. Carbon is the constituent element of steel, and its presence in the steel ball is limited to 1.2%. The steel balls lubricated with GO and rGO grease exhibited significantly higher wt% of carbon (18.5% and 15.35%, respectively), which could be ascribed to the formation of graphene–based tribo–film over the worn scar. The uniform distribution of carbon besides the core elements suggests good quality thin film formation. The EDS spectrum of worn surface greased with GO–ODA grease (**Figure 4.24c**) exhibited nitrogen (5.5 wt%) besides carbon, iron, oxygen, and chromium. The abundance of nitrogen and carbon, and their uniform distribution, revealed the formation of graphene–based tribo–film, which plays crucial roles in reducing friction, subsidizing the wear, and protecting the tribo–interfaces against the severity of material loss, and helps in energy saving.

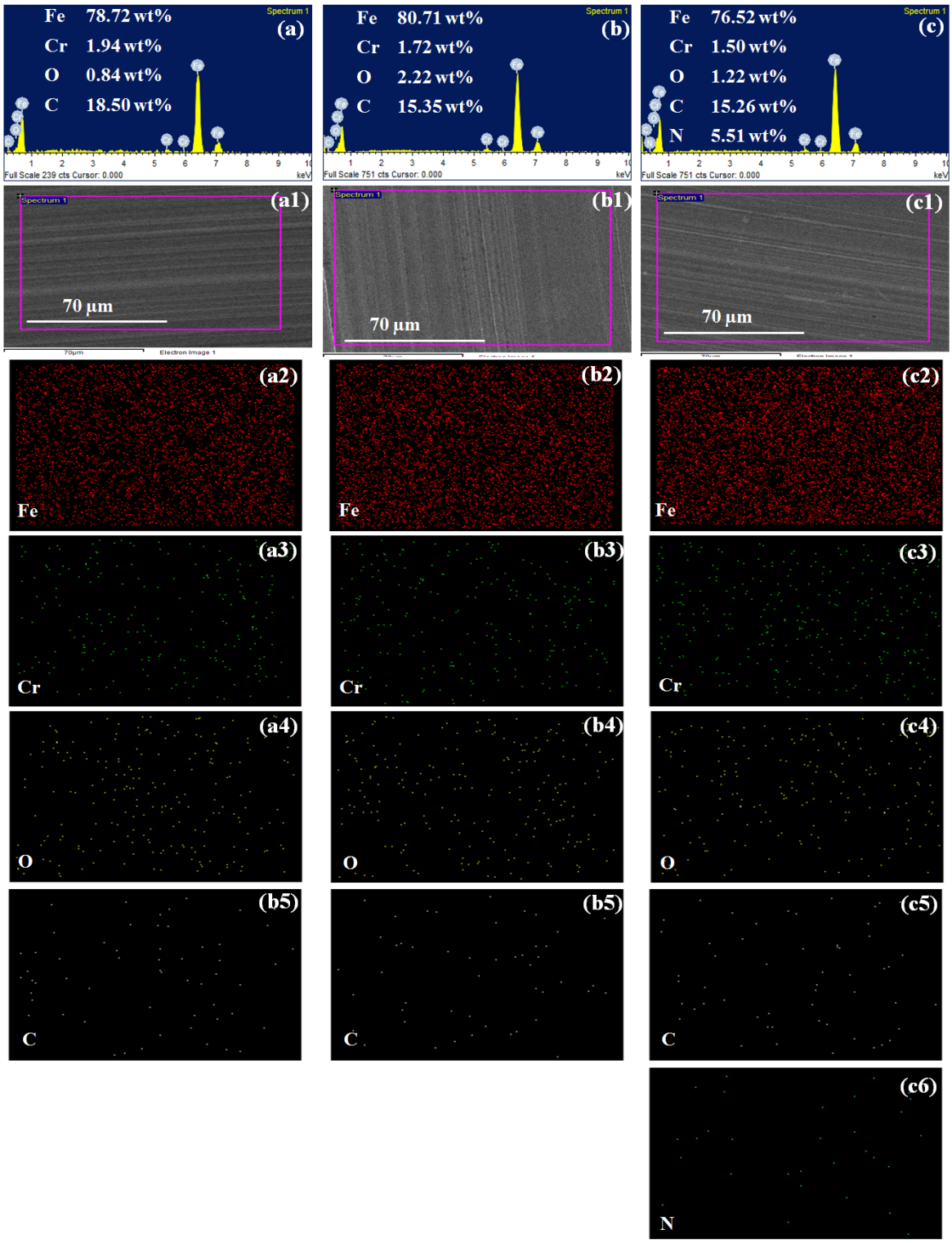

Figure 4.24: EDS spectra with elemental mapping of worn surfaces of steel balls lubricated with (a) 0.01 wt% GO blended grease, (b) 0.01 wt% rGO blended grease (c) 0.05 wt% GO–ODA blended grease. (Applied load: 392 N, test duration: 60 min)

4.8 Tribological performance of greases on SRV–5 machine

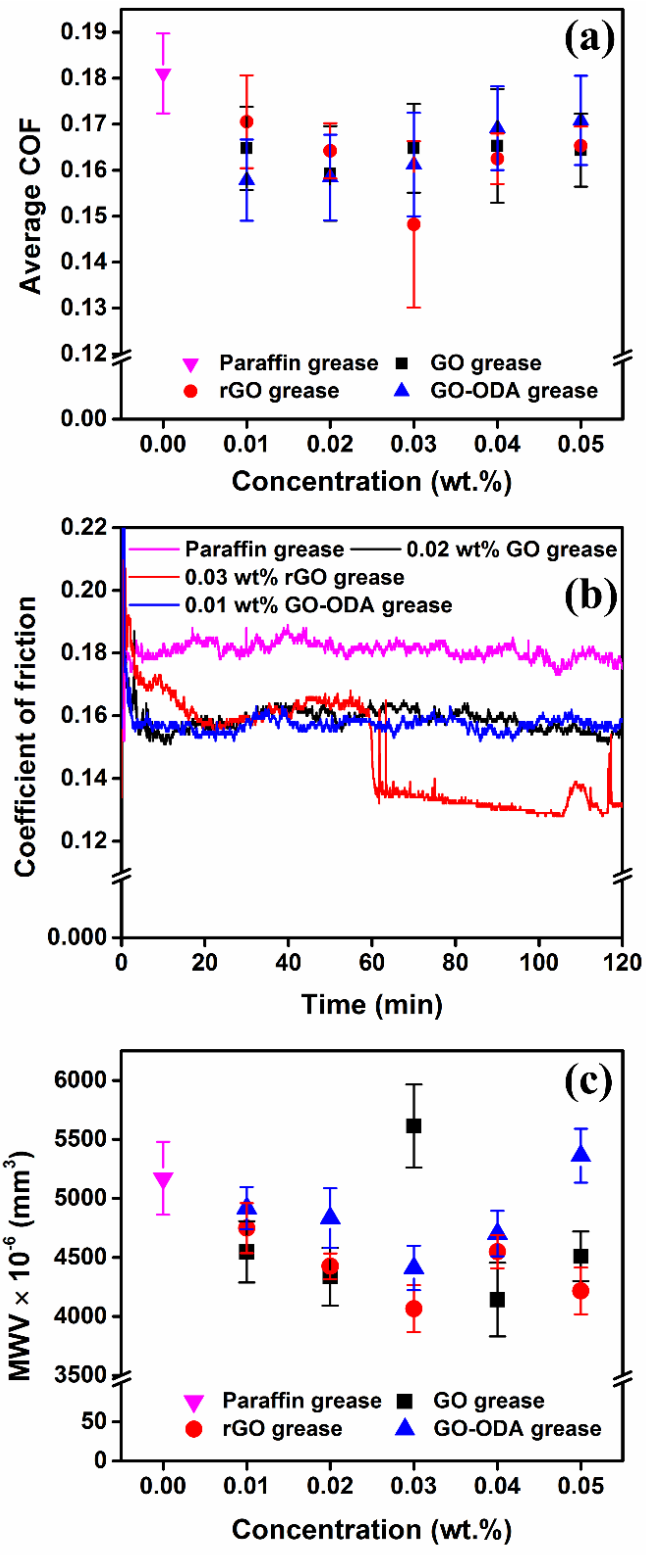

Figure 4.25: Variation in (a) average COF with variable doses of GO, rGO, and GO–ODA in the greases (b) friction profiles with time and (c) MWV of steel tribo–pair lubricated with GO, rGO and GO–ODA greases. (Applied load: 200 N, stroke length: 1 mm, test duration: 120 min)

The SRV 5 test rig was used to assess the tribological behavior of formulated grease according to the ASTM D5707 standard. The variation in average COF and MWV as a function of increasing GO, rGO, and GO–ODA doses are shown in **Figure 4.25**. The paraffin grease exhibited the highest average COF ($\mu = 0.181$) among all the samples. The incorporation of graphene–based nanomaterials as an additive to the paraffin grease decreased the friction. The paraffin grease having 0.02wt% of GO exhibited a maximum reduction (~12%) in the friction. Further increasing doses of GO exhibited a steady rise in the COF. The incorporation of rGO to paraffin grease showed better tribo–performance as compared to that of GO. A 0.03 wt% of rGO showed a maximum reduction in friction (~18%). The GO–ODA, too, improved the tribo–characteristics of paraffin grease. However, the degree of improvement is lesser than that of rGO. A 0.01 wt% of GO–ODA displayed an utmost decrease in friction (~13%). The friction profiles of paraffin grease, 0.02 wt% of GO grease, 0.03 wt% of rGO grease, and 0.01 wt% of GO–ODA grease, are shown in **Figure 4.25b**. The steady friction profiles were maintained after running in–period when a tribo–film is established at the friction pairs. Steady–state profiles indicate that the uninterrupted supply of graphene–based nanomaterials at the friction pairs, which has enhanced the lubrication behavior of the grease. **Figure 4.25c** illustrates the change in MWV for paraffin grease with and/or without variable concentrations of graphene–based nanomaterials. The 0.04 wt% of GO showed a maximum decrease (~20%) in the MWV, whereas 0.03 wt% of GO–ODA and rGO in paraffin grease demonstrated a maximum reduction in MWV, i.e., ~14% and ~21%, respectively. These tribological results suggest that very low doses of graphene–based nanomaterials have a noteworthy potential to boost the tribological behavior of greases. The severity of wear was estimated by calculating the

wear coefficient. **Table 4.5** summarizes the wear coefficient of all the grease samples being studied.

Table 4.5: Wear coefficient of paraffin grease with variable concentration of GO, rGO, and GO–ODA nanosheets

Dose, wt%	Wear coefficient (*k*)			
	Paraffin Grease	GO Grease	rGO Grease	GO–ODA Grease
0.0	0.036	–	–	–
0.01	–	0.032	0.033	0.034
0.02	–	0.030	0.031	0.034
0.03	–	0.039	0.028	0.031
0.04	–	0.029	0.032	0.033
0.05	–	0.031	0.029	0.037

4.9 Study of worn surfaces tested on SRV–5 machine

The SEM images of worn scars on steel discs lubricated with paraffin and graphene–based grease samples are shown in **Figure 4.26**. The wear track width (WTW) on steel disc lubricated with paraffin grease is estimated to be 785 μm (**Figure 4.26a**). The breakdown of tribo–film leads to the seizure of asperities of steel tribo–pair, which results in the gradual removal of material (and micro–pits) driven by adhesive wear. The deep furrows on the worn surface suggest abrasive wear (**Figure 4.26b**). The WTW of worn scars on discs with graphene–based greases were decreased significantly (**Figure 4.26c,e,g**). The rGO grease showed maximum reduction (~14%) in WTW compared to that of paraffin grease. The high–resolution microscopic images of worn surface lubricated with graphene–based greases exhibited comparatively smoother features (**Figure 4.26d,f,h**) with lesser degrees of furrows and micro–pits. These results revealed that GO, rGO, and GO–ODA nanosheets as additives to paraffin grease provide excellent protection to tribo–surfaces.

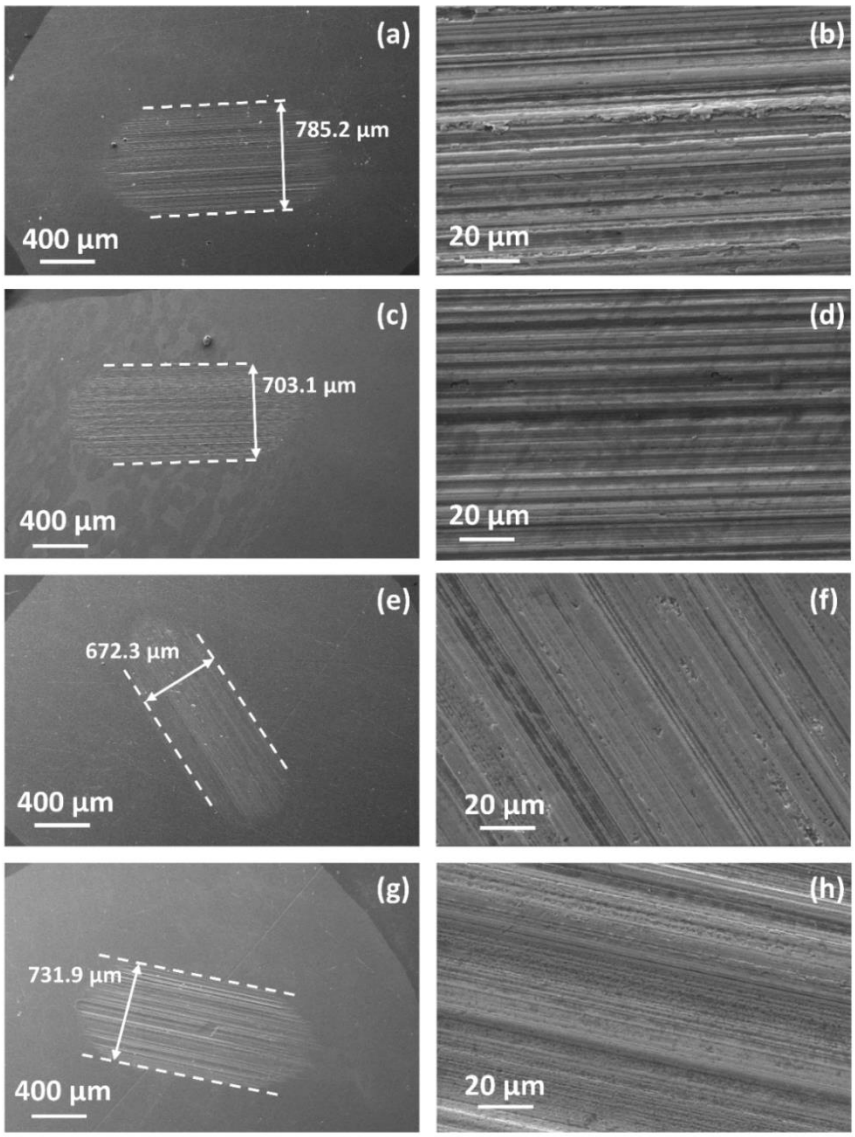

Figure 4.26: Worn surfaces of steel discs lubricated with (a) paraffin grease (b) 0.04 wt% GO blended grease, (c) 0.03 wt% rGO blended grease, and (d) 0.03 wt% GO–ODA blended grease. (Applied load: 200 N, stroke length: 1 mm, test duration: 120 min)

The SEM micrographs of worn scars of steel balls are shown in **Figure 4.27**. The test ball lubricated with paraffin grease displayed maximum WSD (i.e., 737 µm) along with sharp scratches, signifying the adhesion and abrasive wear (**Figure 4.27a–b**). The WSDs were reduced in the presence of graphene–based nanomaterials in the grease. The maximum reduction in WSD (~14%) was found using the rGO grease at the optimized concentration.

Graphene–based nanoadditives have reduced the adhesive wear, and the severity of wear features was also subsidized.

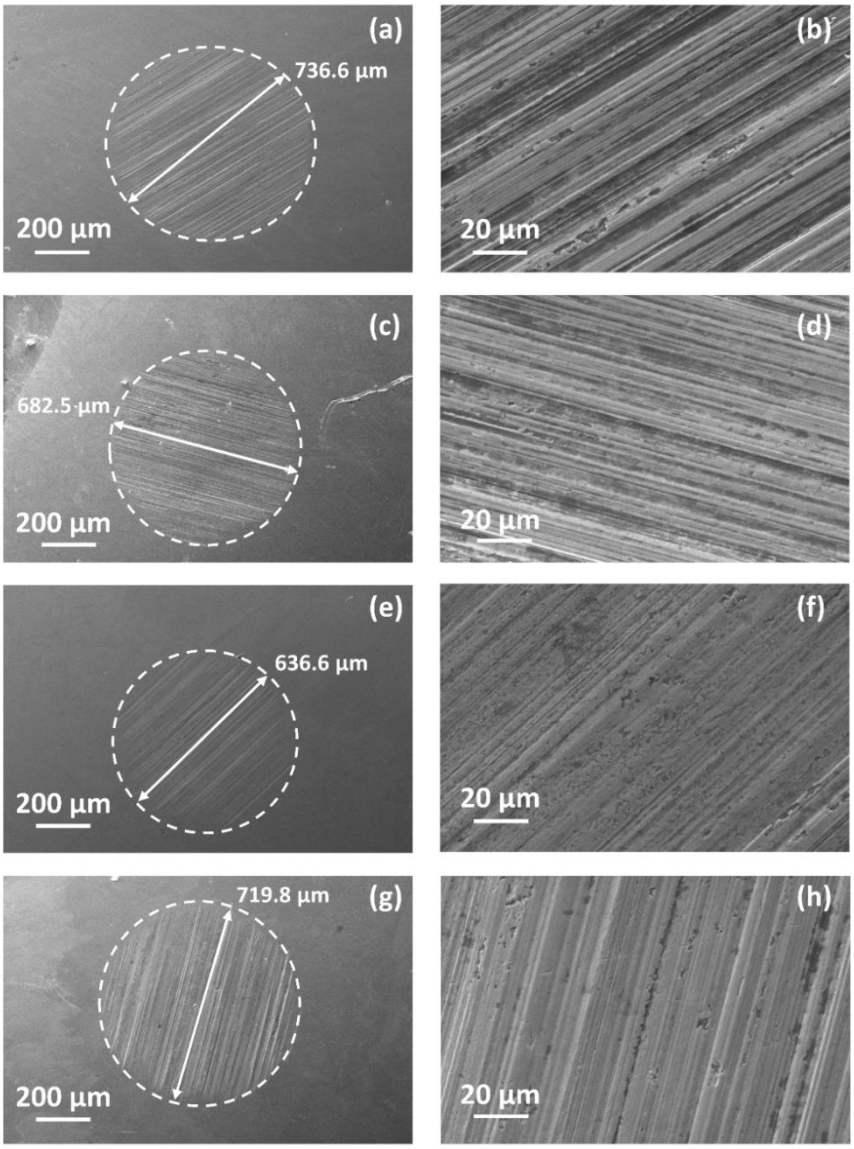

Figure 4.27: Worn surfaces of steel balls lubricated with (a) paraffin grease (b) 0.04 wt% GO blended grease, (c) 0.03 wt% rGO blended grease, and (d) 0.03 wt% GO–ODA blended grease. (Applied load: 200 N, stroke length: 1 mm, test duration: 120 min)

Figure 4.28 illustrates the surface profiles of the worn tracks on steel discs. The pattern of wear tracks was measured in the transverse to the stroke length. These profiles were used for the estimation of Wq of steel discs. The disc lubricated with the paraffin grease (**Figure 4.28a**) showed a maximum loss of material (Wq = 2099 μm^2), which is further supported by **Figure 4.26a–b**. The incorporation of GO, rGO, and GO–ODA to paraffin grease

reduced the Wq, indicating that graphene–based nanomaterials as additives contributed a crucial role in protecting the tribo–interfaces.

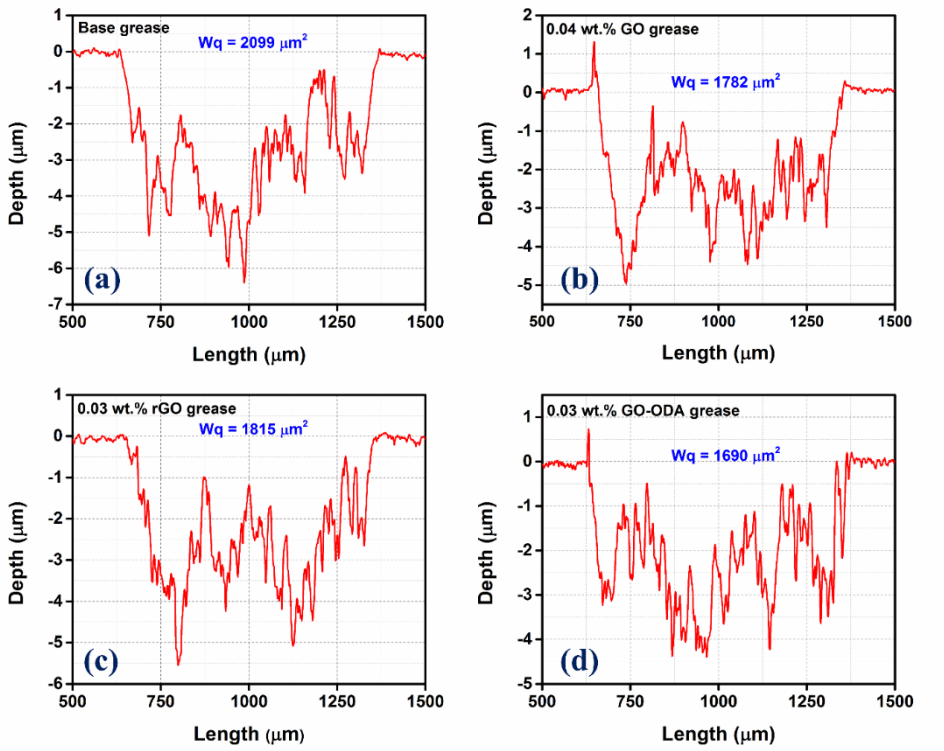

Figure 4.28: Surface profile of worn track developed on steel discs lubricated with (a) paraffin grease, (b) 0.04 wt% GO blended grease, (c) 0.03 wt% rGO blended grease, and (d) 0.03 wt% GO–ODA blended grease. (Applied load: 200 N, stroke length: 1 mm, test duration: 120 min)

The EDS analyses of worn discs and balls were conducted to comprehend graphene–based nanomaterials role in establishing a tribo–film. The SEM micrographs and EDS spectra, comprise the elemental mapping of the corresponding area of worn scars on discs and balls, are shown in **Figure 4.29** and **Figure 4.30,** respectively. The EDS spectra of the steel disc and ball lubricated with paraffin grease exhibited iron, oxygen, and carbon as major constituent elements (**Figure 4.29a1 and Figure 4.30a1**). The 100Cr6 steel has carbon in the range of 0.98–1.2 wt%, but the presence of carbon on the worn surfaces lubricated with paraffin grease has shown more than 7%. The high percentage of carbon on worn surfaces could be attributed to paraffin oil and thickener, hydrocarbon derivatives. The worn

surfaces lubricated with GO–ODA, rGO, and GO greases confirmed the presence of carbon, a characteristics element of graphene–based nanomaterials. Importantly, the presence of carbon has significantly increased to 29.55%, 30.74%, and 21.69% on the worn surfaces lubricated with GO–ODA, rGO, and GO greases, respectively. The high concentration of carbon on the worn area suggests the deposition of carbon–based lubricious tribo–film. Furthermore, worn surfaces GO–ODA lubricated disc and ball exhibited a strong signature of nitrogen (**Figure 4.29d1 and Figure 4.30d1**), a characteristic element of ODA grafted on the GO. The presence of oxygen on all worn surfaces could be attributed to oxidative events during the tribo–tests.

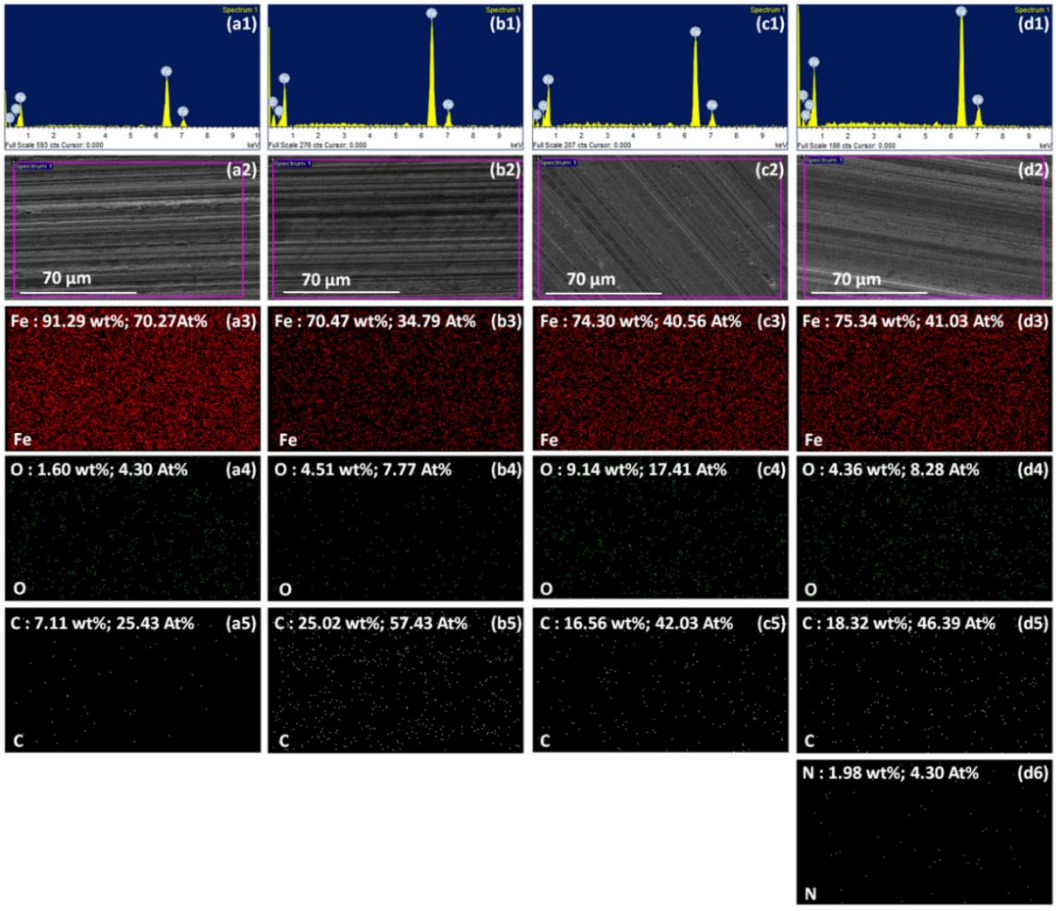

Figure 4.29: EDS spectra along with elemental mapping of worn steel discs lubricated with (a1–a5) paraffin grease, (b1–b5) 0.04 wt% GO blended grease, (c1–c5) 0.03 wt% rGO blended grease, and (d1–d6) 0.03 wt% GO–ODA blended grease. (Applied load: 200 N, stroke length: 1 mm, test duration: 120 min)

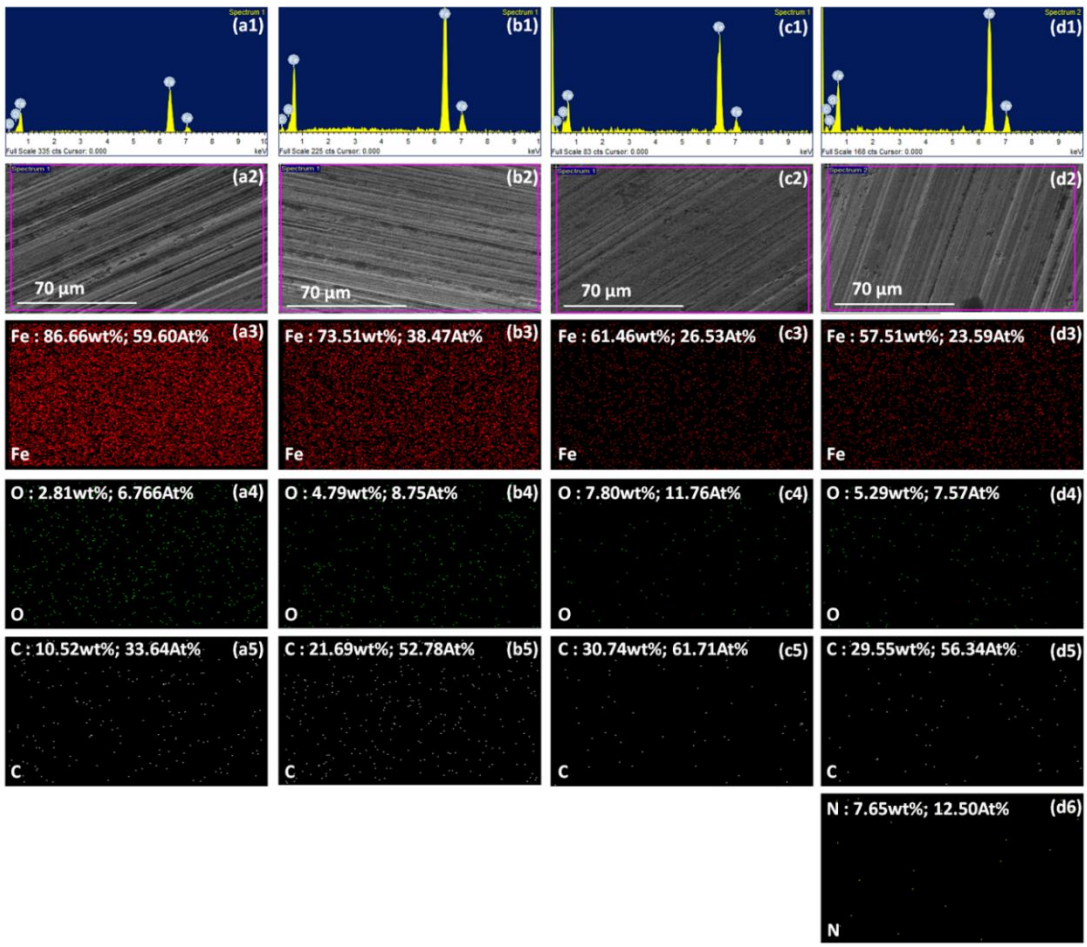

Figure 4.30: EDS spectra along with elemental mapping of worn scars of steel balls lubricated with (a1–a5) paraffin grease, (b1–b5) 0.04 wt% GO blended grease, (c1–c5) 0.03 wt% rGO blended grease, and (d1–d6) 0.03 wt% GO–ODA blended grease. (Applied load: 200 N, stroke length: 1 mm, test duration: 120 min)

4.10 Discussion

The fibrous network of the thickener entraps the lube base oil via van der Walls and capillary interactions (Lugt, 2009). The Hertzian contact stress plays a significant role in establishing a thin film between the tribo–interfaces. The Hertzian contact pressure in the four–ball tester was found to be ~3.4 GPa for steel balls. Whereas the Hertzian contact stress between the disc and the ball in the SRV–5 was found to be ~2.74 GPa. The soap molecules are sheared and squeezed under the high contact stress, which led to the liberation of lube base oil and entrapped nanoadditives. The grease thickener formed a

lubricating thin film in 40–100 nm over the friction surfaces, which separated the interacting steel bodies (Cann, 2007). The discharged lube base oil along with nanoadditives and thickener lubricate the steel tribo–pair and formed a protective tribo–film (Fan et al., 2018). The shear rate and shear duration govern the behavior of the grease. As the shear rate increases, the viscosity of grease is decreased, and the shear thinning of the grease is observed (Singh et al., 2017). During the degradation of the grease, the lubricating oil bleeds from the fibrous soap structure along with the nanosheets into the contacting surface. These nanosheets play a crucial role in reducing the friction and wear behavior of the contacting surface. The temperature–induced at contact pressure between the friction pairs was less than the melting point of the grease. Due to the adverse effect, the heat generated in the grease becomes soft; thus, bleeding of oil from the grease increases. The grease bleeding process plausibly released the lube oil along with nanosheets which lubricated the rubbing surface. The probability of melting the grease is increased with the increment of contact pressure.

The MoS_2 nanosheets trapped in the soap matrix of paraffin grease are released during the Hertzian stress and participated in establishing the tribo–film. The soap molecules in the paraffin grease matrix are squeezed under such high contact stress, shear rate, and temperature, facilitating the exposure of trapped MoS_2 nanosheets in the grease matrix to the contact surfaces, which establishes the boundary film (Sahoo and Biswas, 2014). This film plays a vital role in the enhancement of tribo–performance of the mating surface. The tribo–film developed between the friction pairs is due to the presence of base oil and thickener. The nanosheets and grease molecules are sheared and pressed between the rubbing surfaces. Therefore, nanoadditives and grease fibers get deposited on the worn surface. The paraffin grease without the additive shows higher COF and MWV in

comparison to the nanosheets blended grease, revealing that nanosheets play a vital role in forming a thin protective layer between the contacting surfaces.

During the sliding of the mating surface, the new surfaces are continuously formed and exposed to the surrounding environment and thus leading to the formation of the thick film. The thickness of the oxide and other chemically reacted layers depends on the reactivity of the materials to the environment, reaction temperature, and time (Stachowiak and Batchelor, 2013). Typical thicknesses of these layers range from 10 to 100 nm, although much thicker layers can be formed. The presence of lubricant and nano–additive causes the formation of solid reaction layers that help in surface protection. Furthermore, Hu et al. (2010) have investigated the tribological performance of liquid paraffin with MoS_2 as an additive in a four–ball tester. The worn area analysis the formation of an oxidation film comprising of Fe_2O_3, MoO_3, $Fe_2(SO_4)_3$, and other compounds. In the present result, the worn surface showed the presence of oxygen functionalities as traces of MoO_3 and adsorbed water molecules besides the trapped moisture in the microstructural matrix of grease. Therefore, the distribution of oxygen was found on the worn surfaces (**Figure 4.23**). The oxidation of steel surface and iron oxide formation facilitated the interaction with MoS_2 nanosheets and promoted the interaction via Mo–O and S–O linkages under the frictional test (Tannous et al., 2011). Furthermore, the dangling sulfur atoms in the outer layer of MoS_2 nanosheets are prone to interact with the iron surface under the Hertzian–stress. Gradually, MoS_2 is believed to be deposited on the mating interfaces, further confirmed by the elemental mapping (**Figure 4.23**). However, it is very difficult to isolates the all–plausible interactive pathways behind the formation of tribo–induced boundary thin film, where Hertzian–stress, oxidation of steel surfaces, the formation of third bodies by chemical reactions between the grease, worn particles of iron/iron oxide, and MoS_2, the interaction between the iron surface with dangling sulfur atoms of MoS_2 nanosheets, and

so on govern the quality of tribo–film. The plausible events develop the tribo–induced boundary thin film, which protects the contact interface against the material loss and facilitates the sliding for a reduction in friction. Nanosheets entrapment between the friction pairs reduces the real area of contact. The decrement in the real area of contact causes a decrease in the contact pressure, and hence the friction force is proportional to the real area of contact. The interfacial shear strength of the layered material between the mating surfaces influences the frictional force. The MoS_2 lamellae either deposited or as a constituent to a developed tribo–film on the mating interfaces and furnished the low resistance to shear because of a lamellar slip in the weak inter–planer regions of MoS_2 nanosheets (Kumari et al., 2017). The crystalline nature and strong covalent bonding within a MoS_2 lamella furnish high mechanical strength and thermal stability. In contrast, the dangling sulfur atoms in the MoS_2 lamellae show good affinity with metal surfaces to form the thin film under the tribo–stress. The MoS_2 reacts with steel surface via S–O, Mo–O, and Fe–S linkages and forms the protecting tribo–chemical thin film (Tannous et al., 2011). This film protects the contacting surfaces against direct asperity to asperity contact and protects the friction pairs against wear.

The released graphene sheets interacted with tribo–interfaces and the thickener molecules and furnished the complex tribo–chemical thin film, which enhanced the lubricious properties (Sahoo and Biswas, 2014). Therefore, graphene–based nanomaterials blended greases furnished low friction and MWV compared to the paraffin grease. The molecular lamellae of GO, rGO, and GO–ODA nanosheets facilitated the shearing under the Hertzian contact stress. The ultralow thickness and thorough blending of graphene–based nanomaterials in the grease matrix ensured the uninterrupted supply at the contact interfaces and lubricated the tribo–pair. The graphene–based nanoadditives are believed to delaminate under the high sheared stress and deposited on the rubbing surfaces. The

shearing of graphene–based nanomaterials in the grease with a deposited thin film at the interacting surfaces has decreased the friction. However, the degree of reduction is found to be governed by the crystalline structure of GO–based nanomaterials. Graphene–based nanosheets form a complex tribo–film under sliding stress. The nature of the thin film being formed is governed by several factors, including contact stress and the presence of surface–active additives, the crystalline nature of graphene–based nanomaterials, and the composition of tribo–interfaces. Both surface active thickener and graphene–based nanomaterials formed a complex tribo–film under the boundary lubrication contact. The presence of graphene–based nanomaterials in tribo–film revealed its significant role. It furnished the low resistance to shear, which is governed by the crystalline structure of graphene nanosheets. It has been revealed that graphene–based materials at both macro (Mungse and Khatri, 2014) and nanoscale (Berman et al., 2015; Zeng et al., 2018) studies have enhanced the lubrication properties. The rGO with a characteristic interlamellar spacing furnished minimum resistance to shear; thus, rGO blended grease showed maximum reduction in wear and friction compared to GO–ODA and GO greases. Furthermore, the deposited graphene thin film avoided the direct contact of metallic asperities, resulting in no severe wear furrows, and scratches on the worn surfaces, and it subsidized the wear. The real contact area was reduced due to graphene–based nanosheets between the interacting surface (Gupta and Harsha, 2018b). The atomic lamellae of graphene are linked with each other by the weak van der Waals interaction and furnish low resistance to shear under the sliding stress; thus, graphene displays a good reduction in friction. However, graphene oxide exhibits a significant degree of oxygen functionalities and structural defects and sp^3 hybrid sites in the basal plane. These oxygen functionalities form the hydrogen bonds in the interlayer space, which results in higher binding energy between the atomic thick lamellae. Therefore, oxygen functionalities destroy the shearing

properties of graphene–based materials and increased friction (Berman et al., 2015). Among all samples, rGO with the lowest degree of oxygen functionalities in the basal plane is believed to furnish high–shearing due to weak van der Waals forces. Therefore, rGO–blended grease exhibited the utmost decrease in friction.

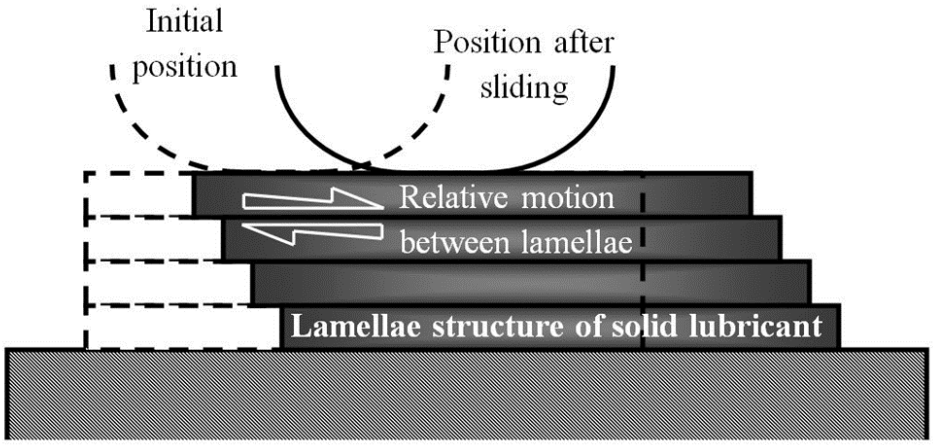

Figure 4.31: Plausible lubrication mechanism revealing the role of nanosheets under the tribo–stress

The crystal structures of MoS_2 and graphene are shown in **Section 1.6**. The tribological characteristics of the lubricating film of MoS_2 and graphene–based materials are very similar. MoS_2, a transition metal dichalcogenide, and graphene, a two–dimensional (2D) honeycomb lattice structure of sp^2–hybridized carbon exhibit, lamellar structure. The molecular lamellae are held together by the weak van der Waals interactions, facilitating the shearing under the sliding stress and reducing the friction (Cizaire et al., 2002; Onodera et al., 2009). **Figure 4.31** demonstrates the lubrication mechanism of solid lamellae. The 2D nanomaterials effectively interact with contact–interfaces under the tribo–stress and form the protective tribo–film of low shear strength, results in the enhancement of tribological properties (Mungse et al., 2015; Tannous et al., 2011). The high mechanical strength, excellent shearing properties, and good affinity to interact with tribo–interfaces

under the high contact–stress make the MoS_2 and graphene–based nanomaterials superior to the conventional additive lubricants/greases.

4.11 Summary of the chapter

The MoS_2, MoS_2–ODT, GO, rGO, and GO–ODA nanosheets have been synthesized successfully. The TEM images of MoS_2, MoS_2–ODT, GO, rGO, GO–ODA exhibit the lamellar structure. The paraffin grease was formulated with paraffin oil (base oil) and 12–lithium hydroxystearate (thickener) via an in–situ technique. Then, the paraffin grease was doped with MoS_2, MoS_2–ODT, GO, rGO, and GO–ODA nanosheets in variable concentrations separately. The tribological performance of various greases was evaluated through a four–ball tester and SRV–5 test machine as per ASTM standard. Further, the viscous flow test and small–amplitude oscillatory shear test was carried out within linear viscoelastic range to investigate the rheological performance of various grease samples. The results showed that the rGO doped grease exhibited maximum reduction in the friction, wear, and energy consumption among all samples, and it was attributed to low shear strength, driven by the weak van der Waals interaction between their adjacent lamellae.